Electrochemical Corrosion Investigation of Structural Materials in Molten Fluoride Eutectic Salts

A Thesis

Presented in Partial Fulfillment of the Requirements for the

Degree of Master of Science

with a

Major in Chemical Engineering

in the

College of Graduate Studies

University of Idaho

By

Matthew Lawson

Approved by:

Major Professor: Haiyan Zhao, Ph.D.

Committee Members: D. Eric Aston, Ph.D.; Krishnan Raja, Ph.D.

Department Administrator: Dev Shrestha, Ph.D.

August 2023

Abstract

This thesis investigates the corrosion behavior of structural materials when exposed to molten fluoride eutectic salts using electrochemical techniques. The research objective is to rank and screen metal structural materials for nuclear reactors based on their performance in determining physical properties, including impedance, corrosion rates, and polarization in FLiNaK salt at 700 °C. The ranking and screening process involved evaluating the materials' performance in these tests and establishing a relative hierarchy. Criteria such as lower corrosion rates, higher impedance values, and increased polarization resistance to corrosion were considered during the analysis. Electrochemical impedance spectroscopy (EIS), Tafel, and polarization resistance (Rp) measurements were conducted for nickel, stainless steel 304, stainless steel 308, Inconel 600, Inconel 617, and HastelloyN. The results revealed variations in the physical properties and corrosion mechanisms of the alloys based on their composition. The EIS analysis provided insights into the corrosion mechanisms and interface properties of the materials, contributing to the development of improved materials in future work. Additionally, the Rp measurement indicated the materials' resistance to corrosion. The findings of this study have significant implications for the design and selection of materials for future high-temperature applications involving molten fluoride eutectic salts, including Gen-IV nuclear reactors and molten salt batteries. The knowledge gained from this research contributes to the development of more durable and efficient materials by delivering important physical property data of metals in molten salts at high temperatures. This knowledge can facilitate the use of these materials as structural components capable of withstanding harsh environments, ultimately enhancing the reliability and safety of high-temperature systems up to 700 °C.

Acknowledgments

I would like to express my deepest gratitude to my major advisor, Dr. Haiyan Zhao, for her unwavering support, invaluable guidance, and immense expertise throughout the entire duration of my research. Her dedication to excellence and passion for our field have been instrumental in shaping my academic journey. I am also grateful to my committee members, Dr. Eric Aston and Dr. Krishnan Raja, for their insightful feedback, valuable suggestions, and constructive criticism. Their expertise and scholarly input have significantly enhanced the quality of this thesis.

I would like to extend my sincere appreciation to the Center for Advanced Energy Studies (CAES) and its exceptional staff for providing me with a conducive research environment. I am especially grateful to Rocky McDowell, the manager of CAES, for his support and coordination, as well as Kristi Moser-Mcintire, the safety officer, and Dustin Hughes, the assistant safety officer, for ensuring a safe and secure working environment.

I am indebted to Dr. Indrajit Charit for graciously allowing me to utilize his metal cutting and polishing equipment. His generosity and expertise have been instrumental in the successful completion of certain aspects of this research. Lastly, I would like to express my heartfelt gratitude to Dr. Djamel Kaoumi, the Principal Investigator of the NEUP project (#19-17173), for providing me with the invaluable opportunity to be a part of this groundbreaking research endeavor. His vision, leadership, and continuous support have been instrumental in shaping my research experience.

In addition, I would like to acknowledge the contributions of all the individuals who have provided their guidance, assistance, and encouragement throughout my research journey. Your support has been invaluable and deeply appreciated.

Dedication

This thesis is dedicated to my best friend, Rowdy. For twelve years, you have been my loyal and steadfast friend, standing by my side through the highs and lows of this academic journey. Your unwavering presence and unconditional love have provided me with solace and inspiration during the most challenging times. You have been my constant source of comfort and motivation. In moments of doubt and exhaustion, your wagging tail has reminded me to persevere and embrace the joy of the present. Whether it was our long walks in nature or our quiet moments of reflection, you have been a gentle reminder of the importance of balance and taking care of oneself. You have shared in my triumphs and offered solace during setbacks, always providing a loving presence that transcends words. Your simple yet profound way of being has taught me the essence of empathy, compassion, and unconditional love. As I conclude this chapter of my academic journey, I dedicate this thesis to you as a testament of my gratitude and appreciation. Thank you for your unwavering support, your playful spirit, and your ability to make every day brighter. You have enriched my life in countless ways, and I am forever grateful to you.

Table of Contents

List of Tables

List of Figures

Chapter 1: Introduction

1.1 Research challenges and motivation

Next generation of nuclear reactors (Gen IV) has several proposed reactor types, one of which utilizes molten salts. The molten salt reactor (MSR) utilizes a coolant comprised of molten salts, affording high temperature operation at low pressure[1]. One mixture of coolant salts proposed for Gen IV operation is called FLiNaK, which is a eutectic salt composed of 46.5 % lithium fluoride, 11.5% sodium fluoride, and 42% potassium fluoride. This eutectic mixture melts at 454 °C and boils at 1570 °C, offering a wide operating temperature range. FLiNaK was not nominated to be a fuel-bearing coolant,[2] but it is still considered a viable and cheaper intermediate coolant to transfer heat from the fuel-bearing coolant loop to a turbine loop. The next step is to find a structural material that will resist corrosion from high temperature FLiNaK salts enough to be sufficient for long term duration.

Corrosion here is caused by the high temperature FLiNaK attacking a metal. Reaction A shows a general example of the metal corrosion mechanism:

$$M \rightarrow M^{n+} + ne^{-} \qquad [1]$$

where M is any metal or alloy, M^{+} is the oxidized metal or alloy species, and e^{-} is the electron that has switched to a more preferrable host. For FLiNaK, the more preferrable host will be from the fluoride ions. Gibbs free energy of formation values greatly assist in understanding stability of a chemical or chemical species in any system. A study at the Savannah River National Laboratory[3] showed the ranking of Gibbs free energy of formation values (kJ/mol/F_2) of various structural materials combined with fluoride ions as LiF < NaF < KF < AlF_3 < MnF_2 < CrF_2 < CrF_3 < FeF_2 < CoF_2 < FeF_3 < NiF_2 < MoF_3, where the more negative the more stable it is. If the alloys are created to be homogenous and corrosion is uniform, the most stable alloys that resist corrosion in FLiNaK will be composed of molybdenum, nickel, and iron since those are the top three most stable compounds according to the Gibbs free energy ranking. Most of the atoms present in alloys will lose at least two electrons during the corrosion process while some will lose three. Since corrosion is expected to occur on the structural materials tested here, the corrosion potentials (E_{corr}) will all be expected to be negative.

Corrosion testing has historically been performed through an immersion test. The samples are cleaned and weighed before and after a set immersion time, anywhere from 100 to more than 1,000 hours, in the environment of interest. Instead, electrochemical corrosion testing is employed here, which assists in determining corrosion rates, resistances, impedances, and equivalent circuit models

in as little as 4 to 5 hours. The much shorter time required for data acquisition and analysis allows for more materials to be tested in a shorter time period, which is helpful as the demand for finalizing Gen IV reactors increases proportionally to the demand for renewable energy technologies. Three electrochemical corrosion testing techniques—electrochemical impedance spectroscopy (EIS), tafel, and linear polarization resistance (LPR), respectively—are employed to study impedance and equivalent circuits, corrosion rates, and resistances. These techniques allow for materials to be ranked from best to worst to determine their suitability as structural materials for the Gen IV MSRs.

1.2 Research objectives and tasks

The objective is to rank several structural materials by their physical properties in eutectic FLiNaK salt at 700 °C within the first 4 hours of immersion. At the specific time immersion intervals of 0.5, 1, 2, and 4 hours, electrochemical measurements will be taken to determine each structural materials physical properties, such as polarization resistances, corrosion rates, and impedances. These physical properties will be determined by linear polarization resistance, Tafel, and electrochemical impedance spectroscopy techniques which are commonly used in corrosion studies. The polarization resistance values indicate the structural materials resistance to oxidation events from the molten salt. The corrosion rates, which will be reported in units of millimeter per year, will help to show how long a structural material will last in a 700 °C FLiNaK environment. The impedance values determined here will lead to deeper understanding of the changes in the electrical behavior of the structural materials, which are not limited to resistance and capacitance, but also ion transport, interfacial reactions, and the formation of passive layers. The task is to add electrochemical corrosion study data to the scientific literature pertaining to metals and alloys polarization resistance to 700 °C FLiNaK salts.

1.3 Research scope

The study focused on employing the three electrochemical corrosion testing techniques to determine electrochemical properties for nickel wire, stainless steel 304 coupon, stainless steel 308 wire, Inconel 600 wire and coupon, Inconel 617 coupon, and HastelloyN coupon in eutectic FLiNaK salts at 700 °C within a 4-hour period of immersion in an inert argon environment. Two samples (SS304 and SS308) with high chromium content (~20%) were included but further samples with high chromium content were not sought out as chromium was shown to readily form chromium fluorides. Future samples for further testing would include high nickel or high molybdenum content as those

fluorides do not readily form. The final goal of the project will be a ranking of the tested structural materials as the best samples out of this batch that would be best suited for structural material use for high-temperature molten salt applications, at least for Gen-IV nuclear reactors but possibly molten salt batteries and other possibilities not yet discovered. The top ranked materials could also be further tested with potentiodynamic polarization tests to further understand passivation zones or metastable pitting events, long term immersion test to ensure thoroughness of corrosion through understanding mass loss, and scanning or transmission electron microscopy to determine structure defects and compare that with impedance data, determine porosity of sample, and acquire composition of corrosion layer with EDX.

Chapter 2: Literature Review

Section 2.1 Introduction to Electrochemical Impedance Spectroscopy

This section seeks to review the corrosion of metals or alloys utilizing a technique called electrochemical impedance spectroscopy (EIS). EIS utilizes alternating current (AC) to probe corrosion in situ, which has been a great benefit to understanding corrosion. Three-electrode systems are mostly discussed which probe corrosion in various types of aqueous and molten salt electrolytes. Equivalent circuit models are used to fit Nyquist plots and Bode plots. Scan frequencies are employed from high to low, and span ranges of 100 kHz down to 0.01 Hz and perturbation signals are generally slightly above the open circuit potential. The equivalent circuit models provide understanding on the whole system with components to be able to separately determine the electrolyte resistance, any oxide layer charge transfer resistance and/or capacitance, and the corroding analytes charge transfer resistance and/or capacitance.

Starting with an EIS analysis of carbon steel in an alkaline solution, Fratuer et al[4]. sought to use EIS to investigate the corrosion of a mild C15 steel in 0.1 M NaOH. Therefore, the working electrode was C15 steel, the counter electrode was a platinum grid, and the reference electrode is a saturated (K_2SO_4) mercury sulphate electrode (MSE-E^0 = 0.64 V/SHE). Open circuit potential (OCP) was monitored for 60 hours, which is when steady-state corrosion was reached. The frequency scan range was 10^{-3} to 10^5 Hz and was performed at room temperature. The article shows the Bode plots, both experimental and simulated. The magnitude of impedance is shown to decrease as frequency increases until around 10^3 where impedance is no longer changing as frequency increases. The phase angle shows steady state behavior from 10^{-2} to 10 Hz and then steeply declines to another steady state value between 10^4 to 10^5 Hz. The regions of steady-state behavior in the phase angle vs frequency Bode plot show that the input did not change once it has gone through the entire system, which is relevant because it says the system is stable at these frequencies. Lastly, it shows the equivalent circuit model generated for the system which is Re-[C_{dl}-$Z_{F,O2}$]-[PLM_{oxide}-$R_{OX,e}$]. The Re component is typically used to express electrolyte resistance. The rest of the circuit is used to describe the working electrode and the oxide layer seen to form on top. The oxide layer was mathematically determined by EIS and there was visual determination used to verify this via X-ray photoelectron spectroscopy. The capacitance values of the double layer (Cdl) were able to be quantified, as well as the impedance of the electrolyte, and the resistance of the oxide layer. The resistance of the oxide layer shows its resistance to a charge transfer in the electrolyte environment, which is useful for showing the protective oxide layer.

As the previous article explored corrosion in an aqueous environment, the next one explores corrosion on aerospace vehicles, as they are not exempt from corrosion. The testing of corrosion of aerospace vehicles performed by Usman et al[5]. Here AA 2024-T3 wrought alloy was used as a working electrode in a 0.46 M sulfuric and 0.533 M tartaric acid corrosive environment at 37 °C. To complete the three-electrode system, the counter electrode was platinum, and the reference electrode was a silver-silver chloride electrode cell. The frequency range for EIS was conducted from 100 kHz to 0.01 Hz with the perturbating signal of 5 mV (rms). The experiment also conducted a salt spray test and utilized an SEM for surface characterization.

The article shows one of several Bode plots, no Nyquist, that were obtained from EIS fitting. This figure represents the three types of tests done, immersion (IMM), hybrid (HYB), and salt spray (SSP) and how the corrosion of the analyte changed between the three types of corrosion tests when monitored by EIS. The first Bode plot shows very little deviation of corrosion between the experiments and the only steady state for corrosion appears around the 10 Ω-cm^2, 1k Hz range to the 50k Hz range. The phase angle portion of the Bode plot shows instability for the immersion test in the very low frequency range, and none of the other corrosion tests are showing similar results until the 500 mHz range, and then there is consistency between types of tests for the duration of the scan. Aside from the multiple Bode plots, no Nyquist plots were generated, no equivalent circuit model was found.

The experiment concluded that the optical surface scans and the EIS scans showed that between the three techniques used, IMM, HYB, and SSP, there was little to no effect of the types of exposure had on the corrosion of the alloy. Unless the determination of a corrosion rate was skimmed over, that piece of data was not discussed or calculated either. This goes to show that EIS can be utilized in unconventional ways, even if it is just to show analytically that there is no difference in how the corrosion is applied, either immersed or sprayed.

Moving from aerospace corrosion to monitoring corrosion in molten salt environments for solar cell power (CSP) has been of interest lately to Encinas-Sanchez et al[6]. who are trying to further the science and understanding behind solar cells that utilize molten ‘solar’ salts at 580 °C for producing electricity. The solar salts have ideal heat transfer properties but are composed of a corrosive composition of 60% $NaNO_3$/40% KNO_3 mixture of salts. This experiment went with a two-electrode system where the working electrode is the sample that’s proposed to be used that will be containing the salt, P91 steel and the counter electrode is another sample of P91 steel, which also served as the reference electrode. The solar salts and electrochemical system were contained by an alumina ceramic crucible, which is a good system for containing molten salts due to its resistance to the corrosion effects but would make a poor structural type of material.

Two corrosion experiments were run simultaneously, the immersion testing and the EIS testing. Electrodes were weighed before and after immersion testing at intervals of 0, 24, 72, all the way up to 1000 hours, which is the classical way of measuring corrosion and reporting a penetration depth per unit of time, typically mm/yr. SEM and XRD scans were also performed to help support the corrosion rate analysis of the immersion testing. EIS was performed by using a sinusoidal voltage of 10 mV and utilized a frequency range of 50 kHz to 10 mHz. Nyquist plots when scanned at 2 hours and after 1000 hours of immersion time. Unfortunately, the article does not show all the scans overlayed on top of each other to show how the impedance changed with time. No Bode plots are shown, and no mention of error analysis from the model found to fit the data. By monitoring the OCP and getting a current back, that current was equated as corrosion current and was used to calculate a corrosion rate which started at 23 μm/yr and approached steady state by around 500 – 1000 hours to obtain approx. 300 μm/yr corrosion rate.

From molten salt corrosion to acid rain corrosion, this next experiment, the effects of acid rain on alloys are being studied[7] and EIS is used to understand the corrosion under cyclic wet-dry conditions. A three-electrode system is utilized where the working electrode is the 2024-T3 alloy of interest, the counter electrode is a platinum circle, and the reference electrode is a saturated calomel electrode (SCE). EIS frequency scanned from 1 KHz to 0.01 Hz with a perturbation signal of 5 mV. The electrolyte (acid rain) in this case was comprised of deionized water that had the pH adjusted to between 3.5 and 4.5 with sulfuric acid and potassium hydroxide.

Nyquist plots obtained at pH 3.5 and sees more impedance on the real axis and less impedance on the imaginary axis. The equivalent circuit model is also shown, where two CPEs are used, an Rp, and a Rt component. Nyquist plots obtained at pH 4.5 with a very typical Nyquist plot creating the ideal half circle plot to easily determine components like Rs and Rt from the graph. The difference between these two graphs is that the pH 3.5 shows a capacitive arc at the high frequency domain from corrosion, forcing the Nyquist plot to deviate from ideal conditions that are displayed in the 4.5 pH region.

Section 2.2 EIS Corrosion and alloys

This second section focuses on specific corrosion of materials like stainless steel and nickel-based alloys and helps to understand diffusion in an electrochemical system using EIS[16]. This paper utilizes EIS to find a diffusion coefficient for aluminum chloride salts into graphite utilizing a eutectic salt mixture of $AlCl_3 - NaCl - KCl$ at 140 °C. The experiment takes advance that since angular frequency (ω) and Warburg impedance are correlated to Fick's law of diffusion. The article shows one of the three Nyquist plots generated from EIS and included an equivalent circuit model to go with it. Utilizing the three Nyquist plots where the only change was the DC offset potential (-1.16, -1.18, and -1.22 V), the flux was then calculated utilizing equation 23, equation 24, equation 25 and subsequently diffusion.

$$Z_f = \frac{\delta E_1}{\delta I_f} + \frac{\delta E_2}{\delta I_f} \quad [2]$$

$$\frac{\delta J_{ion}}{\delta E_2} = \frac{\xi_{ion}}{1+\zeta_{\text{ion}}\left(\coth\left[\frac{d\left(\frac{j\omega}{D_{ion}}\right)^{0.5}}{(j\omega D_{ion})^{0.5}}\right]\right)} \quad [3]$$

$$\zeta_{ion} = K_{ion}^1 \exp\left[b_{ion}^1 (E - E^0)\right] K^{-1} \exp[b^{-1}(E - E^0)] C_{ion} \quad [4]$$

In conclusion, from these equations, one single diffusion coefficient was published, which was for aluminum chloride ions diffusing into graphite in the proposed molten salt mixture at 140 °C, the diffusion was calculated to be 2.8×10^{-10} cm/s. This study was also able to discuss and show anomalous diffusion, what totally blocking and totally absorbing boundary conditions are, and the main criterion for identifying anomalous diffusion type behavior, which is heavily reliant on the slope of the high-frequency line generated in Nyquist plots.

After monitoring corrosion of alloys with EIS in a molten salt environment, the corrosion of stainless steel 316, by Sarvghad et al[17]. focuses on measuring corrosion with electrochemical and spectroscopic methods. NaCl, Na_2SO_4, K_2CO_3, Li_2CO_3, and Na_2CO_3 salts were mixed to form a eutectic molten salt. The three-electrode system, at 700 ºC, utilized platinum sheets for all working, counter, and reference electrodes. EIS and potentiodynamic polarization scans were conducted vs OCP. EIS was scanned in 100 kHz to 100 MHz ranges. Table 1 shows the data collected during the experiment, giving corrosion potential, corrosion current, and polarization resistance for platinum in the molten salts. Three different molten salt mixtures were experimented on. Provided this was a

thermal energy storage experiment, the article still found a formation of films on the surface of the alloys in all molten salt experiments. This begs the question as to whether they cleaned their electrodes between runs.

Table 1. Supporting data for polarization plots obtained during this experiment. Picked for the results of E_{corr}, I_{corr}, B_A, B_C, and Rp values.

Salt mixture	E_{corr} (mV)	I_{corr} (μA·cm^{-2})	B_a (mV/decade)	$\|B_c\|$ (mV/decade)	R_p (Ω·cm^2)
Chloride sulfate	−466	74	288	262	113
Chloride carbonate	−24	247	221	313	20
Ternary carbonate	−539	6	56	143	225

Afterwards, the article goes on to show some electrochemical testing of the SS316 samples. The article shows the standard Nyquist plot of imaginary vs real impedance, as well as just one of the two typical bode plots, showing the log-log plot of impedance's magnitude vs frequency. It seems to be quite rare that there is no circuit model accompanying the Nyquist bode plot combination, but this article does not report a circuit model. One important note though is that the Nyquist plots are somewhat like ones seen in the FLiNaK experiment. Typically, Nyquist plots create a half circle as discussed previously but it was nice to see other experiments have somewhat similar plots to data seen in the results section of this thesis. The lack of extra data processing (the circuit model) is of concern though. I tried looking for the EIS parameters used, to see any similarities, but none were mentioned.

From spectroscopic corrosion monitoring methods, coupled with EIS, to HITENC molten salt corrosion monitoring, the next article[7] focuses on the corrosion of stainless steel 316 in HITEC molten salts. HITEC molten salts are a mixture of sodium nitrate, sodium nitrite, and potassium nitrate (40,7,53 wt% respectively). There were three temperatures investigated, 450, 600, and 680 ºC and the corrosion was tested with potentiodynamic polarization and EIS. Even though the ASM V13A recommends using a 0.1 mV/s scan rate, this article elected to go with a 20 mV/min (0.3 mV/s) scan rate, which netted some very good data. The EIS data was run between 0.01 Hz and 100 kHz, which is also recommended by the ASM 13A, except they used a two-electrode system for EIS, this

is not uncommon but not typically used. The discussion of potentiodynamic polarization discusses some corrosion mechanisms of:

$$M = M^{2+} + 2e^{-} \quad [5]$$

$$\frac{1}{2}O_2 + 2e^{-} = O^{2-} \quad [6]$$

Which is very broad, but their discussion talks about this reaction and the use for potentiodynamic polarization method. The journal shows their tafel analysis and had a much more interesting trend-showing graph than ours did. Albeit the graphs do look nice, the experimenters performed this corrosion test in an air atmosphere. Looking through this paper to find out how they accounted for the extra corrosion from the air atmosphere.

Continuing with molten salt and alloy corrosion, the article written by Patel et. al[42]. covers high-temperature corrosion tests of alloys: Nimonic 80A, Inconel 718, and Inconel C-276. They use two techniques, potentiodynamic polarization electrochemistry and immersion methods, to perform the corrosion studies at 680 ºC. The article reported corrosion potential (V) values for 80A, 718, and C-276 at -0.278,-0.303, and -0.206, respectively. Also included were the corrosion currents (mA/cm^2) reported at 0.6599, 0.1404, and 0.0029, respectively. Afterwards, corrosion rates are reported at 0.5, 0.45, 0.05 mm/year, respectively. Most of the discussion revolves around SEM picture differences of before-and-after pictures of the alloys and theoretical reasons for why C-276 showed better corrosion resistance than the other metals.

Some differences in this experiment, opposed to the current FLiNaK project, is that this project utilized platinum sheet as a quasi-reference electrode and a platinum crucible. the water and oxygen levels in the argon atmosphere gloveboxes were also below 1 ppm. The glovebox at CAES usually is above that value in the 2~5 ppm range, depending on the day. The reference electrode and crucible differences would theoretically only account for open circuit potential differences, not specifically corrosion rates. Even though the corrosion rates for the FLiNaK project were seen to be in the thousands of um/yr range, they could very well be in the same range as these, since the units for the corrosion rates here are in mm/yr. The inconel C-276 and Nimonic 80A, albeit they are nickel-based alloys, can’t be as easily compared as Inconel 718 can to Inconel 600. Oddly enough, even though nickel-based alloys are focused in this paper, there is no pure nickel experimented on. Nor is there even mention of what pure nickel’s corrosion looks like compared to something like Nimonic 80A, which is 76.6% nickel.

One of the most important points taken from this article was the idea of using immersion time coupled with electrochemical impedance spectroscopy (EIS) to observe corrosion rates. This article did not specifically EIS and immersion method, but this is where the idea to do this to the current FLiNaK project came from. This article utilized immersion method coupled with tafel analysis to support the claims of chromium depletion near the surfaces of the alloys was the main reason for the significant loss weight.

Maintaining the review trend of molten salt and alloy corrosion, the next article published by Hua Ai et al[18]. discusses severe corrosion of a Ni-W-Cr alloy in fluoride molten salts. The two nickel-based alloys used are Ni-26W-6Cr and GH3535. FLiNaK molten salts were also used as electrolyte (46.5mol% LiF, 11.5mol% NaF, 42mol% KF). The article utilizes the immersion method, electrochemical methods, and DFT to conclude the results and discussion of data. The article shows the Nyquist plot obtained for tungsten and molybdenum from EIS. The data presented here is very good work and can easily be referenced in discussion of data for our FLiNaK paper due to its similar results and circuit model.

After the EIS modeling, the discussion section includes reaction mechanisms with fluorides, water, and a metal. It's interesting that this article even discusses these reactions because they are working in FLiNaK salts at around 700 °C most of the time and at that temperature, water would find it very difficult to be in the salt dough. They mention water impurity in the salts, but it seems farfetched that would be the case.

$$H_2O + 2\,F^- = O^{2-} + 2\,HF \quad [7]$$

$$H_2O + F^- = OH^- + HF \quad [8]$$

$$M^0 + n\,HF = MF_n + \frac{n}{2}H_2 \quad [9]$$

Carrying on with alloys corroding in molten salts, the next article, electrochemical study of Ni-based alloy GH3535's corrosion in FLiNaK salts at 700 ºC, was done by Wang et al[20]. This paper performs potentiodynamic polarization methods, as well as utilizes EIS methods to observe the corrosion of their nickel-based alloy. This paper has A LOT of data, discusses potentiodynamic polarization measurement techniques, polarization resistance, solvent resistance (Rs), EIS, SEM analysis of corroded alloy GH3535 and many other aspects of electrochemical corrosion of nickel-based alloys. The SEM and EDX type of analysis were able to determine things like cross-sectional morphologies and etching of their alloy. Interestingly enough, the GH3535's chemical composition

appears to have approximately 70% nickel, with a notable 17% of molybdenum and the rest of the ~13% falls off into the various other metals. Given that the alloy is 70% nickel, the published charge transfer resistance (Rt) is in the range of 260-440 Ω-cm^2 for a pure argon atmosphere and 100-120 Ω-cm^2 with just the addition of 5% water. The Rt drops off quickly here when as little as 5% of an oxidizing agent is introduced. An interesting idea to pursue would be what the FLiNaK results would look like without the 1-3 ppm of O_2 or H_2O in the system.

This paper will be a great reference to utilize when comparing data with other papers. Some corrosion potential and currents were reported in Table 2, which would provide a decent comparison to Inconel, but not great. The article shows an example of how they displayed EIS Nyquist and bode plots, but it is not limited to just this one. The article concludes with a discussion of chromium and the preferential dissolution of Cr^{3+} creating a Cr-depleted zone along their alloy. When thinking of any possible chromium depletion in the system, this will be a great reference.

Table 2. Electrochemical data obtained during Tafel analysis for the GH3535 alloy at 700 °C.

Electrochemical parameters obtained from the potentiodynamic polarization curves of GH3535 at 700 °C in molten (Li,Na,K)F under Ar and Ar-5%H_2O, respectively.

	b_a ($mV\,dec^{-1}$)	b_c ($mV\,dec^{-1}$)	E_{corr} (mV vs. Ni/NiF_2)	I_{corr} ($\mu A\,cm^{-2}$)
Pure Ar	203	176	−432	108
Ar-5%H_2O	265	279	−430	374

Pressing on with molten salt corrosion shows Inconel 718, for corrosion behavior, was studied via EIS[8]. The experiment utilized molten salts consisting of $Na_2SO_4, 80\ V_2O_5 - 20Na_2SO_4, NaVO_3$, and natural ash from a power plant. The three-electrode system was utilized for the EIS experiment where the working electrode was the alloy inconel 718, counter electrode was a platinum wire, and the reference electrode was also a platinum wire. An interesting note here is that the EIS measurement was taken 0.5 hrs AFTER the corrosion potential was established. EIS was taken from 10 kHz to 1 mHz. The article shows three of the Nyquist plots obtained during EIS with the three temperatures experimented on. These Nyquist plots mostly show half circle trends. This is a normal trend seen in EIS studies. Whoever is performing the analysis here can quickly calculate Rp and Rs values. When the EIS is not in a half circular form, modeling must be done to determine those parameters. The article also discusses three different corrosion processes as well. “Under charge transfer control”, “under charge transfer and diffusion control”, and “when alloy is covered with a protective salt layer”. These three corrosion processes could probably be investigated more.

Next, more molten salt corrosion tests were performed[9] in FLiNaK salts at 550 – 750 ºC on Inconel 625, Inconel 617, Inconel 600, Incoloy 800, Incoloy 800 HT, Hastelloy N, and Ni 220. EIS and Tafel analysis was employed for corrosion characterization and EIS results for all the alloys, just at 650 ºC. Since impedance is the same concept as resistance but for alternating current systems, the higher the impedance the higher the polarization resistance, which is seen in this paper. Incoloy 800 HT performed phenomenally well. They also experimented on Inconel 600, so we could very well compare results with this paper directly. They generated an equivalent circuit model for not just Inconel 600 but the same model was used for every single alloy. This is difficult to believe, plus it's a very large equivalent circuit model. The paper here performed experiments on various alloys and at various temperatures ranging from 550 to 750 °C. There are not many graphs showing an overlay of how the data changed with each temperature. This paper has some interesting data, but I find it lacking in quite a few areas, especially since the areas they are lacking are the areas I would like to compare our data to.

Chapter 3: Methods and Materials

3.1 Methods

3.1.1 Electrochemical impedance spectroscopy

The first technique used in a series of three electrochemical techniques is a nondestructive technique known as electrochemical impedance spectroscopy (EIS). As with all spectroscopies, a signal from the electromagnetic spectrum is applied to the sample and the change in the signal received is used for analyses. The signals (frequencies) used here were from 100,000 to 0.1 Hz. EIS produces three graphs and the first one is called Nyquist, which shows imaginary versus real impedance. As the frequency is generated from alternating current, both imaginary and real components are calculated and displayed. The Nyquist plot shows how imaginary impedance (Z'') changes with real impedance (Z'). Real, imaginary, and magnitude of impedance are shown in the following relation:

$$|Z|^2 = (Z')^2 + (Z")^2 \quad [10]$$

and frequency dependent impedance is given by the following relation:

$$Z(\omega) = Z' - jZ" \quad [11]$$

where $Z(\omega)$ is the impedance of the system defined by an angular frequency (ω) and j is the imaginary number, since i is used to represent current. A major downside to Nyquist plots is that there is no frequency shown, even though each impedance value is based on a specific frequency.

Since each value of impedance was generated by a specific frequency, the next two Bode plots help support the Nyquist plot. The Bode plots can be plotted together on a 3-axis plot with a small amount of data, but often come in a pair, depending on the amount of data taken. One plot will show the magnitude of impedance versus frequency and then the phase angle versus frequency. The phase angle is a result of the difference of imaginary and real impedance values, shown in the following relation:

$$\tan(\phi) = \frac{Z"}{Z'} \quad [12]$$

Plotting the phase angle versus frequency shows which frequencies were the most out-of-phase in the system.

Another type of analysis in EIS is the equivalent circuit modeling. Equivalent circuit models allow for a more comprehensive view of the system, breaking it down into specific circuits with various components, such as an inductor, resistor, capacitor, constant phase element (CPE), Warburg elements, and more. Equivalent circuit modeling then goes one step further and determines the values of each component, allowing for determination of the resistance of the electrolyte, the resistance of a passivation layer, the capacitance of an alloy, etc. The equivalent circuit modeling done on these alloys is accompanied by chi-square error values and sum of square error values, which can be found in Appendix A.

3.1.2 Tafel

A destructive technique allows for instantaneous corrosion rates to be calculated by extrapolating data from potential vs log current graphs, known as tafel plots. Tafel is a destructive technique because it forces the working electrode to corrode by scanning into the region positive of E_{corr}. The scan is linear and starts -0.25 V vs OC and ends the scan at 0.25 V vs OC. Ending the scan at a positive voltage vs the corrosion potential forces the working electrode to polarize, hence the technique is destructive. The tafel regions on a tafel plot are linear and found on both the anodic and cathodic branches. Once an equation of a line is determined for each tafel region, the slopes (β) are taken used to determine the corrosion current (i_{corr}) and can are shown in the following equation:

$$i_{corr} = \left(\frac{1}{2.3\ R_p}\right)\left(\frac{\beta_a\beta_c}{(\beta_a+\beta_c)}\right) \quad [13]$$

where β_a is the tafel slope for the anodic branch, β_c is for the cathodic branch, and Rp is the polarization resistance in Ω-cm^2. The area value from Rp is the geometrical surface area of corrosion measured post experiment. Once i_{corr} is calculated, the next step for tafel analysis is the corrosion rate calculation. The corrosion rate is reported as penetration depth over time in the units of millimeters per year (mmpy). The equation for corrosion rate (CR) is:

$$CR = \frac{i_{corr}\cdot K\cdot EW}{d\cdot A} \quad [14]$$

where K is a constant[15] of 3272 mm (A-cm-year), A is the geometrical surface area of corrosion in cm^2, EW is the equivalent weight of the working electrode being corroded in units of gram, d is the density of the working electrode in units of g/cm^3, and i_{corr} is the corrosion current using the unit of amp.

3.1.3 Linear Polarization Resistance

A short-range scan starting at -20 mV vs OC and ends 20 mV vs OC. The principle for LPR utilizes Ohm's law to determine the overall resistance of the system, which is:

$$V = IR \quad [15]$$

$$R = \frac{V}{I} \quad [16]$$

where V is potential in volts, I is current in amps, and R is resistance in Ω. The resistance calculated here is known as polarization resistance (Rp) and is reported in Ω- cm^2. The surface area of the electrode is used multiplied by the observed Rp values to normalize the resistance values. LPR is a useful technique to quickly rank alloys without causing significant damage to them. Although the scan starts negative of corrosion potential and ends positive of the corrosion potential, the end potential is relatively small enough to not cause a lot of corrosion. Equation 37 shows that plotting potential vs current will mean the slope obtained from the plot will be the resistance for the system.

3.2 Materials

A glassy carbon crucible (Sigrauder tapered type T) was used to hold eutectic FLiNaK salts at 700 °C in a jeweler's furnace (KerrLab Auto Electro Melt Maxi). The FLiNaK was comprised of 43.82 g lithium fluoride (99.99%, Alfa Aesar, lot# 10736), 17.54 g sodium fluoride (99.995%, Alfa Aesar, lot# 12964), and 88.64 g potassium fluoride (99.99%, Alfa Aesar, lot# 10980). The glassy carbon crucible was then rotated at 45° to thoroughly mix the salts prior to being heated to 900 °C and held for 2 hours to ensure thorough melting and mixing. All salts were stored and experimented on in an argon glovebox (H_2O and O_2 < 5 ppm), not purified further, and the same salt ingot was used to test all alloys. The potentiostat used was a Princeton Applied Research (VersaSTAT 4) and VersaStudio was used to collect and analyze data. A Kerr Auto Max furnace was used to heat the molten salt with a heating ramp rate of 20 ºC/min for all runs.

The three-electrode electrochemical cell, Figure 10, utilized a glassy carbon rod (Sigrauder, diameter 3 mm) as the reference electrode. A glassy carbon rod (Sigrauder, diameter 3 mm) was used as a counter electrode for the tests with the wire working electrodes and a steel coupon (SynLectro 72Fe/20Cr/8Ni, 10x3x20 mm) was used as the counter electrode for the tests with planar working electrodes. The working electrodes varied from Nickel (wire, 0.5 mm diameter), Alloy 600 (wire, 1 mm diameter), SS308 (wire, 1.59 mm diameter), SS304 (coupon, 3.00 x 0.54 x 9.88 mm), HastelloyN (coupon, 3.00 x 1.03 x 5.43 mm), I617 (coupon, 2.56 x 0.30 x 5.52 mm), and I600 (coupon, 3.01 x 0.55 x 6.76 mm); compositions can be found in Table 1. The counter and working electrodes were suspended in FLiNaK with stainless-steel wires (diameter 0.318 mm). All alloys were wet cut with a diamond blade at 400 rpm from a larger coupon, wet polished with #800 and #1200 grit SiC sandpaper, rinsed with water, sonicated in deionized water for 30 minutes, baked at 200 °C for 2 hours, and left to cool in the glovebox transfer chamber at -25 mmHg.

A) 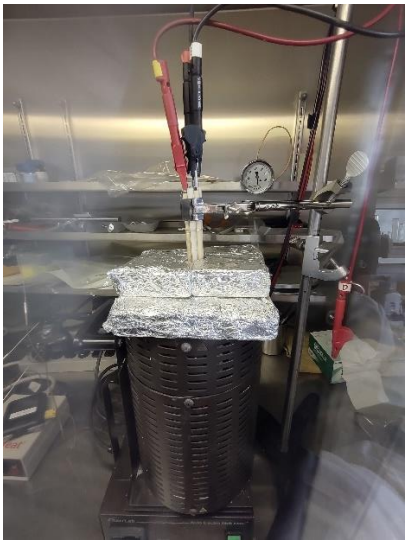 B) 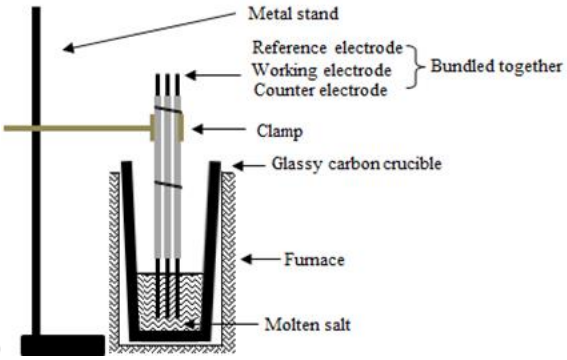

Figure 1. A) Picture of the typical experimental setup used inside the glovebox. B) Cross-sectional schematic of the experimental setup.

Table 3. Material Composition (wt%) for each alloy. I600w = Inconel 600 wire, SS308 = Stainless Steel 308 wire, SS304 = Stainless steel 304 coupon, I617 = Inconel 617,

wt%	Nickel	I600w	SS308	SS304	HastelloyN	I617
C	-	0.05-1.50	0.02	0.042	0.06	0.09
Mn	-	1	1.7	0.84	0.8	0.09
Cr	-	14.0-17.0	20.5	18.23	7	22.29
Ni	99.99	72	10.5	8.09	69.27	52.7
Fe	-	6.0-10.0	66.4	72.32	4	2.17
Al	-	0.3	-	-	0.25	1.13
Ti	-	0.3	-	-	0.25	0.32
Si	-	0.5	0.4	0.39	1	-
Cu	-	0.5	0.21	-	0.35	-
Mo	-	-	0.3	-	16	9.72
Co	-	-	-	-	0.02	11.49
P	-	0.015	0.002	0.032	-	-
S	-	0.015	-	0.003	-	-
N	-	-	-	0.053	-	-
B	-	0.06	-	-	-	-
V	-	-	-	-	0.5	-
W	-	-	-	-	0.5	-

Chapter 4: Results and Discussion

4.1 Nickel wire

4.1.1 Electrochemical Impedance Spectroscopy

Figure 2 shows the Nyquist and Bode plots obtained during EIS analysis for the immersion of nickel in 700 °C FLiNaK salt over 4 hours. The Nyquist plot shows decreases in both imaginary and real impedance. There is a bigger decrease in imaginary impedance over time than the decrease in real impedance over time. The imaginary impedance accounts for the electric current stored in electric fields, which the Nyquist plot shows decreasing over time, so the electric fields capacity is seen to decrease over time as the formation of the passivation layer increases over time. The real impedance, which accounts for the physical dissipation of energy via material resistance, also decreases over time but not as much compared to the imaginary impedance. The Nyquist plot here also suggests diffusion limited behavior since no clear semicircle has formed within the very wide frequency scan range of 0.1 to 100k Hz, which hints toward needing a diffusion circuit model to fit the data, which can be seen as solid lines on the EIS data here. This model is used for the rest of the alloys tested as well and can be seen at Figure 3.

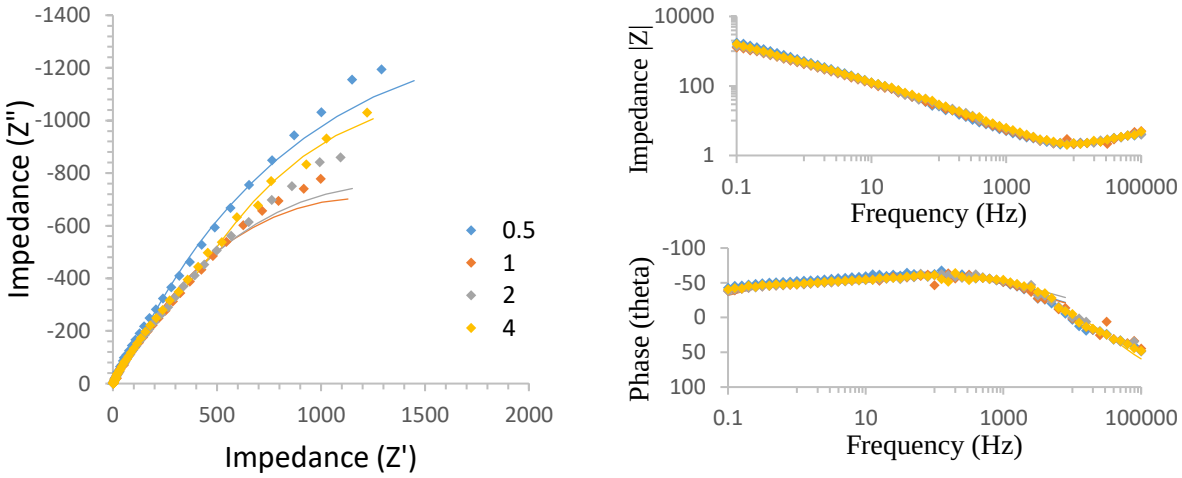

Figure 2. Nyquist (left) and Bode plots (right) for the immersion of nickel in 700 °C FLiNaK for 4 hours.

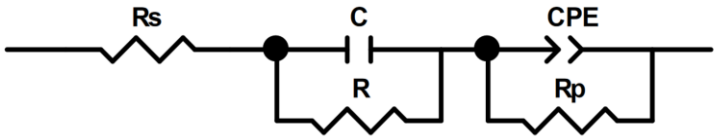

Figure 3. Equivalent circuit model for corrosion mechanisms.

In the case of Nickel, EIS revealed interesting trends over time, shown in Table 4. The Rs exhibited a decreasing trend, indicating enhanced conductivity and reduced hindrance to charge transfer. The increase in the double layer capacitance suggests a growing electrochemically active surface area, possibly due to the formation of corrosion products or dissolution of the alloy. Concurrently, the charge transfer resistance decreased, indicating improved corrosion resistance as the reaction progressed. The constant phase element associated with the double layer capacitance (CPE-T) remained unaffected by the corrosion process. However, the CPE-P (related to passive film capacitance) exhibited a decreasing trend, suggesting the breakdown or thinning of the passive film with time. Overall, the observed changes in the equivalent circuit parameters indicate evolving interfacial processes involving charge transfer and passive film behavior.

Table 4. Nickel EIS data from Corrosion mechanism model.

Hrs	0.5	1	2	4
Chi-Sqr	0.003318	0.005217	0.005155	0.00557
Sum-Sqr	0.31189	0.49035	0.48456	0.53473
Rs(Ω)	1.669	1.834	1.365	1.492
Rs(Error)	0.062621	0.089618	0.091337	0.088342
Rs(Error%)	3.752	4.8865	6.6914	5.921
C(F)	3.12E-04	2.26E-04	2.68E-04	0.000229
C(Error)	2.75E-05	2.75E-05	2.24E-05	2.31E-05
C(Error%)	8.7968	12.18	8.3759	10.069
R(Ω)	50.65	32.56	30.97	30
R(Error)	6.2036	4.2304	3.8882	4.5829
R(Error%)	12.248	12.993	12.555	15.276
CPE-T($S \cdot s^n$)	0.000544	0.000646	0.000648	0.000609
CPE-T(Error)	1.52E-05	2.31E-05	2.09E-05	2.08E-05
CPE-T(Error%)	2.7925	3.5696	3.2309	3.4215
CPE-P(°)	0.71197	0.69111	0.66596	0.67005

Table 4 continued.

CPE-P(Error)	0.005045	0.007224	0.007041	0.006794
CPE-P(Error%)	0.70861	1.0452	1.0572	1.0139
Rp(Ω)	3912	2332	2611	3120
Rp(Error)	289.3	175.52	197.68	283.74
Rp(Error%)	7.3952	7.5266	7.571	9.0942

4.1.2 Tafel

Figure 4 shows the potential vs log current tafel plot obtained during nickels immersion in 700 °C FLiNaK salts for 4 hours. The potential is vs open circuit (OC) and the top of the peak created where current is the lowest is known as E_{corr} in corrosion studies. E_{corr} decreases very slightly from the 0.5 to 4th hour mark, which was seen in its Nyquist plot on the Z′ axis as well. On the top half of the graph, known as the anodic branch, there are passivation zones seen where the current is not changing while potential increases, e.g., the 4th hour yellow line has a zone of no current changing from -0.05 to 0.05 V vs OC. The passivation zone for nickel would be nickel fluoride and is stable up to 0.05 V vs OC. Linear lines were extrapolated from both branches to find the β constants and equation 13 was used to find the current where corrosion occurred (I_{corr}), then equation 14 was used to determine the corrosion rates, which can all be seen in Table 5.

The corrosion rate of pure nickel (99.99% Ni) exhibited a decreasing corrosion rate, from 0.66 to 0.24 mmpy, over time, indicating improved resistance to corrosion in FLiNaK molten salt. The magnitude of corrosion rates were also the lowest from all samples testedThe corrosion rate after one hour was 0.85 mmpy, then continued to decrease to 0.43 mmpy after 2 hours and was found to be 0.24 mmpy after 4 hours of immersion.

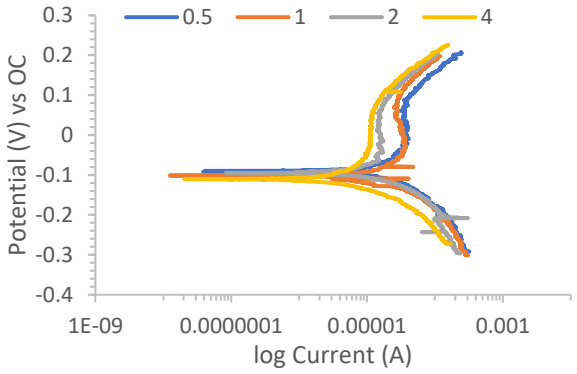

Figure 4. Tafel for Nickel. Density = 8.9 gm/cm^3, area = 0.3217 cm^2, EW = 29.35

Table 5. Corrosion rates, corrosion potentials, corrosion currents, and beta constants for Nickel in 700 °C FLiNaK salts.

Hrs	0.5	1	2	4
CR (mmpy)	0.66	0.85	0.43	0.24
E_{corr} (mV)	-87.66	-97.86	-95.32	-109.31
I_{corr} (uA)	19.65	25.38	12.75	7.11
Cathodic B (mV)	122.64	163.26	104.59	127.32
Anodic B (mV)	127.41	189.09	172.46	127.32

4.1.3 Linear Polarization Resistance

Figure 5 shows the LPR data for nickel immersed in 700 °C FLiNaK for 4 hours. The potential vs current graph shows short linear sweeps obtained at each time interval. Aside from the 2-hour scan, the 0.5, 1, and 4-hour scans are all close in potential. Since LPR is a method concerned with just slope, the steepest slope is seen at the 4-hour mark, followed closely by the 2-hour mark. The data for LPR analysis can be found in Table 6, which shows that within the first hour of immersion, the Rp increased slightly from 565 to 676 Ω. After 2 hours of immersion, the Rp greatly increased to 2543 and then slightly increased after 4 hours to 2698 Ω.

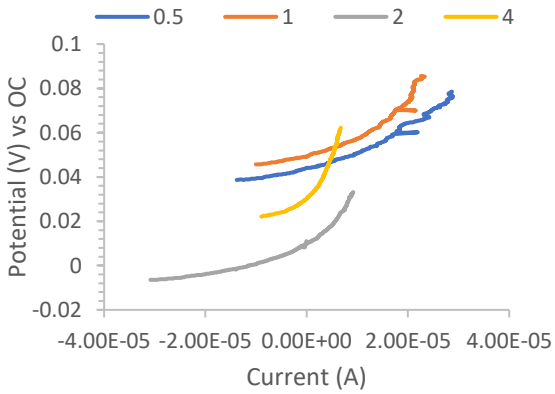

Figure 5. Linear polarization resistances for nickel in 700 °C FLiNaK for 4 hours.

Table 6. Immersion time, polarization resistance, and normalized Rp values for nickel in 700 °C FLiNaK over 4 hours.

Hrs	0.5	1	2	4
Rp	565.254	676.407	2543	2698
Ω-cm^2	181.84	217.60	818.08	867.95

4.2 Inconel 600 wire

4.2.1 Electrochemical Impedance Spectroscopy

Figure 6 shows the Nyquist and Bode plots for the Inconel 600 wire (I600w) when immersed in 700 °C FLiNaK for 4 hours. Starting with the Bode plots, there is no major changes in |Z| vs time nor is there any change in the phase angles vs time, suggesting the I600w material is corroding at a constant rate the entire 4-hour duration, suggesting there was no formation of any fluoride passivation layers or any components of the alloy that immediately pitted out first. The Nyquist plot here also shows very little changes in both imaginary and real impedance over time.

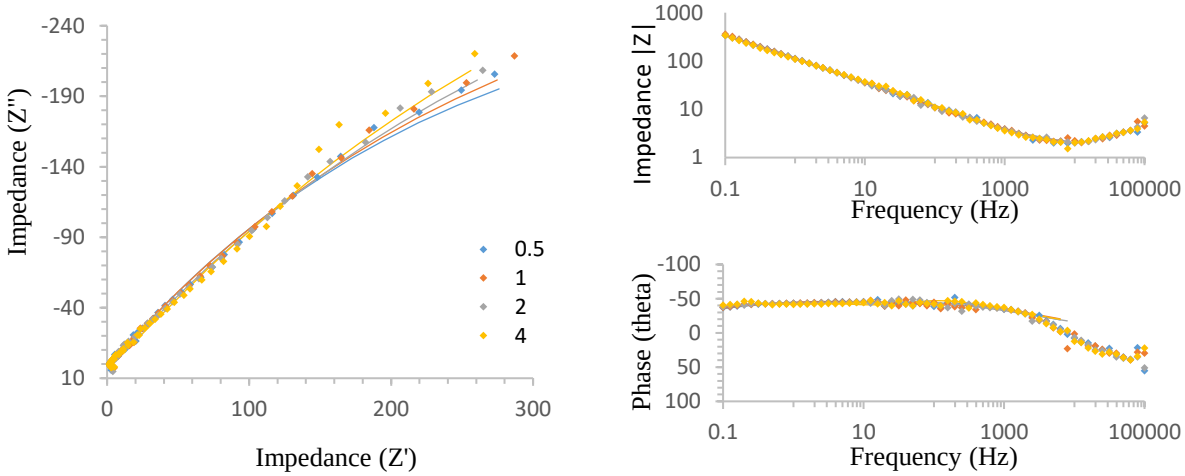

Figure 6. Nyquist (left) and Bode plots (right) for the immersion of I600w in 700 °C FLiNaK for 4 hours.

For I600w, Rs showed a decreasing trend over time, indicating a reduction in the hindrance to charge transfer. Interestingly, the double layer capacitance remained relatively constant, suggesting minimal changes in the electrochemically active surface area. The charge transfer resistance increased progressively, suggesting a higher resistance to corrosion as the reaction proceeded. The constant phase element associated with the double layer capacitance exhibited an increasing trend, possibly indicating alterations in the surface morphology or coverage during the corrosion process. Additionally, the CPE-P remained relatively unchanged, implying the stability of the passive film during immersion. The data for each component at each time interval is seen in Table 7.

Table 7. Inconel 600 wire EIS data from Corrosion mechanism model.

Hrs	0.5	1	2	4
Chi-Sqr	0.003132	0.00367	0.004208	0.004232
Sum-Sqr	0.28817	0.3376	0.39554	0.38932
Rs(Ω)	1.533	1.452	1.511	1.428
Rs(Error)	0.081281	0.089232	0.08388	0.089476
Rs(Error%)	5.3021	6.1455	5.5513	6.2658
C(F)	0.000441	0.000614	0.001956	0.00056
C(Error)	7.91E-05	0.000158	0.000343	8.37E-05
C(Error%)	17.91	25.657	17.525	14.946
R(Ω)	2.367	0.91403	2.905	5.82
R(Error)	0.51561	0.48389	0.86711	0.87092
R(Error%)	21.783	52.94	29.849	14.964
CPE-T($S \cdot s^n$)	0.002911	0.002972	0.003235	0.003365
CPE-T(Error)	9.00E-05	0.0001	0.000108	0.000113
CPE-T(Error%)	3.0921	3.3804	3.3485	3.3691
CPE-P(°)	0.56789	0.55353	0.54423	0.54733
CPE-P(Error)	0.00949	0.010529	0.008077	0.008963
CPE-P(Error%)	1.6712	1.9022	1.4842	1.6377
Rp(Ω)	978	1124	1311	1514
Rp(Error)	109.12	133.24	190.41	245.98
Rp(Error%)	11.157	11.854	14.524	16.247

4.2.2 Tafel

Figure 7 shows the potential vs log current tafel plot obtained during the immersion of I600w in 700 °C FLiNaK salts for 4 hours. The top of the peaks created, where current is the lowest value, on the tafel plot represent the E_{corr} are showing that the corrosion potential decreased as time increased from 0.5 to 4 hours. Since a negative E_{corr} represents corrosion occurring, a positively increasing E_{corr} suggests that less corrosion is occurring as time increases. There are no passivation zones showing in the anodic branch of the tafel though. Since there is E_{corr} changing to the positive direction but no passivation layers forming in the anodic branch, one conclusion could be that one of the specific elements in this alloy were selectively corroding out first, and as that element depleted

off the corrosion area, the corrosion rate decreased. A good way to verify which element might be doing this, for future experiments, is to take small aliquots of the salt out, before each scan is started, and perform an ICP-MS analysis on the salts.

Inconel 600 (Ni-72/Cr-17/Fe-10) displayed a consistent corrosion rate, from 0.56 to 0.53 mmpy, throughout the exposure, suggesting the alloy's ability to maintain its corrosion resistance under the given conditions. This corrosion resistance is due to the high nickel content of the alloy. The corrosion rate after one hour showed 0.78 mmpy, then decreased over time, to 0.65 mmpy after 2 hours, down to 0.53 after 4 hours. Equation 13 and 14 were used to determine corrosion rates and the values obtained from tafel analysis can all be seen in Table 8.

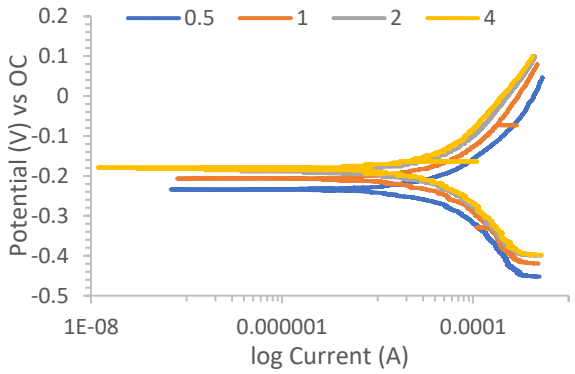

Figure 7. Tafel for Inconel 600 wire. Density = 8.47 g/cm^3, area = 0.496 cm^2, EW = 24.83.

Table 8. Corrosion rates, corrosion potentials, corrosion currents, and beta constants for Inconel 600 wire in 700 °C FLiNaK salts.

Hrs	0.5	1	2	4
CR (mmpy)	0.56	0.78	0.65	0.53
E_{corr} (mV)	-235.48	-209.12	-186.93	-180.44
I_{corr} (uA)	28.96	40.17	33.78	27.30
Cathodic B (mV)	119.32	182.28	152.68	142.19
Anodic B (mV)	119.32	182.28	156.56	142.19

4.2.3 Linear Polarization Resistance

Figure 8 shows the LPR data obtained during the immersion of the I600w in 700 °C FLiNaK during a 4-hour period. Supporting the previous findings of tafel, LPR here shows again that E_{corr} is becoming more positive as time increases for I600w. Since the I600w material has 72% nickel, the

corrosion rate decreasing over time may also be due to a nickel fluoride passivation layer formation but it could be limited by the corrosion products of other materials in the alloy. A good follow-up analysis here would be SEM, as it has the ability to determine which and where each element in the alloy is. The Rp increased from 660 Ω after 0.5 hours to 722 Ω after 1 hour of immersion. Slightly increased to 725 Ω after 2 hours, then quickly decreased to 603 Ω after four hours of immersion. Table 9 shows the Rp values and normalized Rp values obtained for each time interval for I600w.

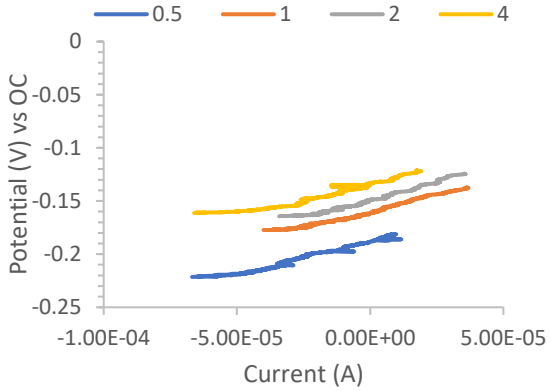

Figure 8. Linear polarization resistances for I600w in 700 °C FLiNaK for 4 hours.

Table 9. Immersion time, polarization resistance, and normalized Rp values for I600w in 700 °C FLiNaK over 4 hours.

Hrs	0.5	1	2	4
Rp	660.585	722.645	725.731	603.761
Ω-cm^2	327.65	358.43	359.96	299.47

4.3 Stainless steel 308 wire

4.3.1 Electrochemical Impedance Spectroscopy

Figure 9 shows the Nyquist and Bode plots for the immersion of stainless steel 308 wire (SS308w) in 700 °C FLiNaK for 4 hours. The Nyquist plot shows a decrease in impedance as time increases. The real impedance decreases from 168 to 125 over the 4 hours of immersion, a total of 43 Ω. The imaginary impedance decreases from -136 to -94, a total of 42 Ω, over the 4 hours of immersion. The real and imaginary both decreased by about the same, suggesting the working electrode experienced uniform corrosion during its immersion time in the FLiNaK. The Bode plot for |Z| vs Hz shows, at low frequency, the impedance decreased over time, from 216 to 156, over the 4 hours.

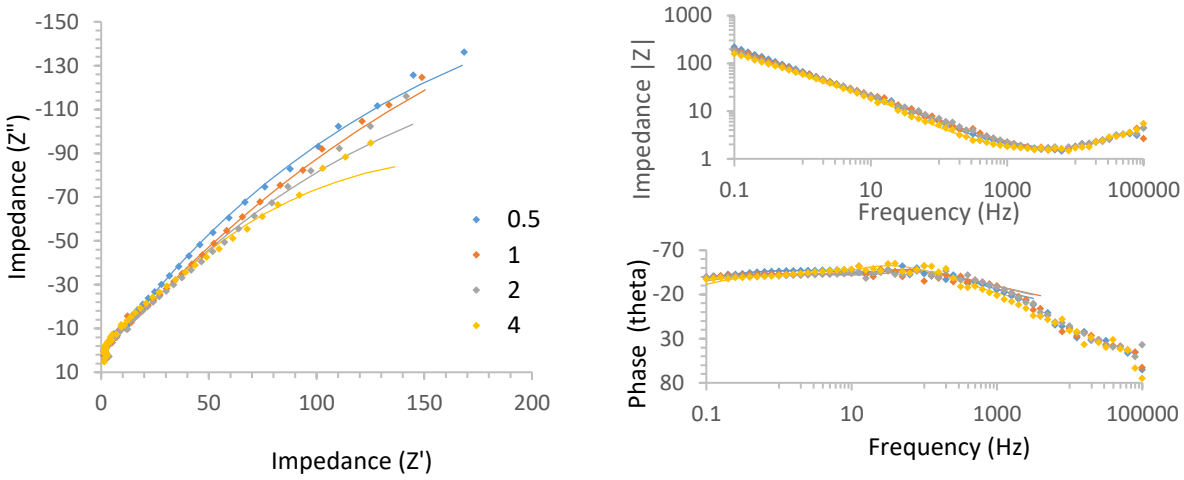

Figure 9. Nyquist (left) and Bode plots (right) for the immersion of SS308w in 700 °C FLiNaK for 4 hours.

For SS308, the Rs remained relatively constant over time, indicating consistent electrolyte conductivity. The double layer capacitance showed no significant changes, suggesting minimal variations in the electrochemically active surface area. However, the charge transfer resistance exhibited a gradual increase, indicating an increase in the corrosion resistance as the reaction progressed. The constant phase element associated with the double layer capacitance displayed an increasing trend, possibly indicating changes in surface roughness or coverage during the corrosion process. On the other hand, the CPE-P remained unchanged, indicating the stability of the passive film during immersion. The data for each component at each time interval is seen in Table 10.

Table 10. SS308 EIS data from Corrosion mechanism model.

Hrs	0.5	1	2	4
Chi-Sqr	0.002449	0.004245	0.003185	0.004016
Sum-Sqr	0.21059	0.37356	0.27388	0.33736
Rs(Ω)	1.3	1.118	1.139	1.321
Rs(Error)	0.04841	0.064652	0.065196	0.053452
Rs(Error%)	3.7238	5.7828	5.724	4.0463
C(F)	0.001668	0.002204	0.001443	0.001851
C(Error)	0.00028	0.000384	0.000213	0.00023
C(Error%)	16.819	17.443	14.793	12.406
R(Ω)	3.258	3.508	3.212	7.311
R(Error)	0.50093	0.80083	0.51922	0.93854
R(Error%)	15.375	22.829	16.165	12.837
CPE-T($S \cdot s^n$)	0.004859	0.005697	0.005733	0.00577
CPE-T(Error)	0.000129	0.00022	0.000186	0.000246
CPE-T(Error%)	2.6549	3.8627	3.2416	4.2682
CPE-P(°)	0.6073	0.55153	0.55909	0.62578
CPE-P(Error)	0.007757	0.008672	0.009294	0.010193
CPE-P(Error%)	1.2773	1.5724	1.6624	1.6288
Rp(Ω)	614.8	791.3	555	324.6
Rp(Error)	64.111	145.62	66.131	31.364
Rp(Error%)	10.428	18.403	11.915	9.6624

4.3.2 Tafel

Figure 10 shows the potential vs log current tafel plot obtained for the immersion of SS308w in 700 °C FLiNaK salts for 4 hours. From the 0.5 to the 4th hour of immersion, the E_{corr} changes from -329 mV to -302 mV, which is a small difference of 27 mV. The 1, 2, and 4th hour of immersion E_{corr} values are close enough to be within small error range of each other, suggesting that steady state corrosion was reached after 1 hour of immersion in FLiNaK at 700 °C. The first half hour of immersion is an unstable data point as well, since the immersion of the electrode bundle, within that time, usually requires the salt to re-reach equilibrium for more than 30 minutes. The anodic branch of the tafel plot here shows no passivation zones were generated during the scans, and the tafel region is

a straight line, showing normal corrosion characteristics. Lines were fit to both anodic and cathodic branches and I_{corr} was extrapolated and calculated.

The corrosion rate of SS308 (Ni-10.5/Cr-20.5/Fe-66.4/Mo-0.3) increased over time, indicating a higher susceptibility to corrosion compared to other alloys tested in FLiNaK molten salt. The corrosion rate remained steady for the first hour of immersion, where the 0.5 hour mark showed 0.98 mmpy and the 1 hour mark showed 0.94 mmpy. After 2 hours the corrosion rate decreased to 0.74 mmpy but then increased to 1.25 mmpy after 4 hours. Equations 13 and 14 were used with the β constants, E_{corr}, and I_{corr} values to determine corrosion rates in mmpy, which can all be seen in Table 11.

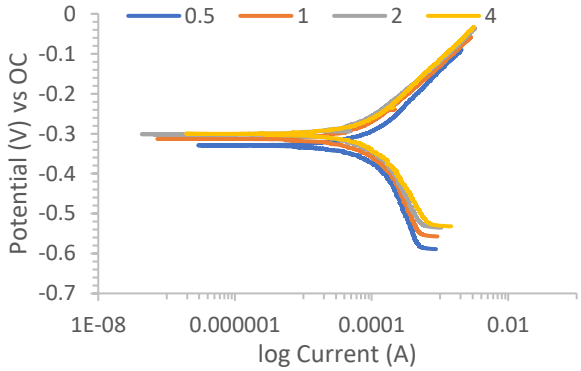

Figure 10. Tafel for SS308w. Density = 7.99 g/cm^3, area = 0.841 cm^2, EW = 25.12.

Table 11. Corrosion rates, corrosion potentials, corrosion currents, and beta constants for Stainless steel 308 wire in 700 °C FLiNaK salts.

Hours	0.5	1	2	4
CR (mmpy)	0.98	0.94	0.74	1.25
E_{corr} (mV)	-328.58	-310.00	-300.65	-301.08
I_{corr} (µA)	79.86	76.79	60.35	102.31
Cathodic Beta (mV)	135.56	148.94	133.77	156.09
Anodic Beta (mV)	135.56	148.94	133.77	156.09

4.3.3 Linear Polarization Resistance

Figure 11 shows the LPR data obtained during the immersion of SS308w in 700 °C FLiNaK for 4 hours. Like the SS308w tafel, the LPR here shows the 0.5-hour mark being more negative than the 1–4-hour immersion marks. The LPR here shows a clear trend as well, that the E_{corr} potential decreases as time increases, showing that the corrosion product decreases as time increases. Rp was found to be 63 Ω after 0.5 hours of immersion, then decreased down to 45 after 1 hour. After 2 hours the Rp was 46 Ω, then decreased slightly to 40 Ω after 4 hours. The Rp values obtained by doing the analysis, as well as the area normalized values, can be found in Table 12.

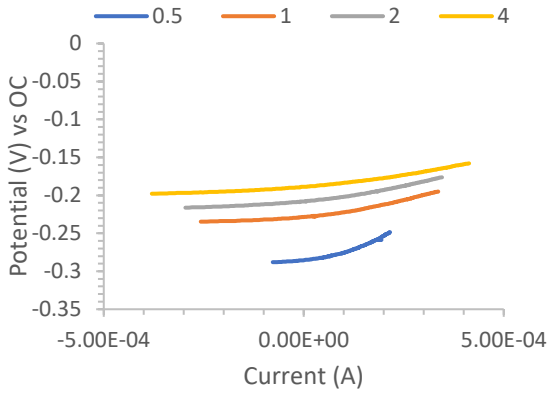

Figure 11. Linear polarization resistances for SS308w in 700 °C FLiNaK for 4 hours.

Table 12. Immersion time, polarization resistance, and normalized Rp values for SS308w in 700 °C FLiNaK over 4 hours.

Hrs	0.5	1	2	4
Rp	63.053	45.261	46.079	40.396
Ω-cm^2	53.028	38.06	38.75	33.97

4.4 Stainless steel 304 coupon

4.4.1 Electrochemical Impedance Spectroscopy

For the rest of the data, there was a switch from cylindrical to planar working electrodes, called coupons. The planar shape was how they were delivered, so some changes made to the system from the previous wire working electrode system was mainly the counter electrode. The previous wire tests utilized a glassy carbon rod for the counter electrode, but the new coupons needed a planar counter electrode to stay consistent with mass transport principles. A SigmaAldrich "Nickel Counter Electrode" was purchased, cut, polished, and hung in the same fashion as the new coupons. Another change is that corrosion was monitored out to the 5th hour, but any comparisons of materials will still utilize the 4th hour of immersion. The extra 5th hour data point was taken to further understand if any steady state behavior was seen or if any passivation zones formed slightly later for each coupon.

Figure 12 shows the Nyquist and Bode plots for stainless steel 304 coupon (SS304c) in 700 °C FLiNaK for 5 hours. The low frequency real impedance values are all in a small region of 65 to 80 Ω whereas the 5th hour of immersion shows a real impedance value of 102 Ω. The Nyquist plot shows that the impedance does not have a significant increase or decrease over time, suggesting there is no significant increase or decrease to corrosion and it remains steady. The |Z| vs Hz bode plot shows the same trend as the Nyquist plot in that the magnitude of impedance does not change greatly over time. As expected, an increase in frequency shows a decrease in impedance which leads to the electrolyte impedance value beyond the 1000 Hz region.

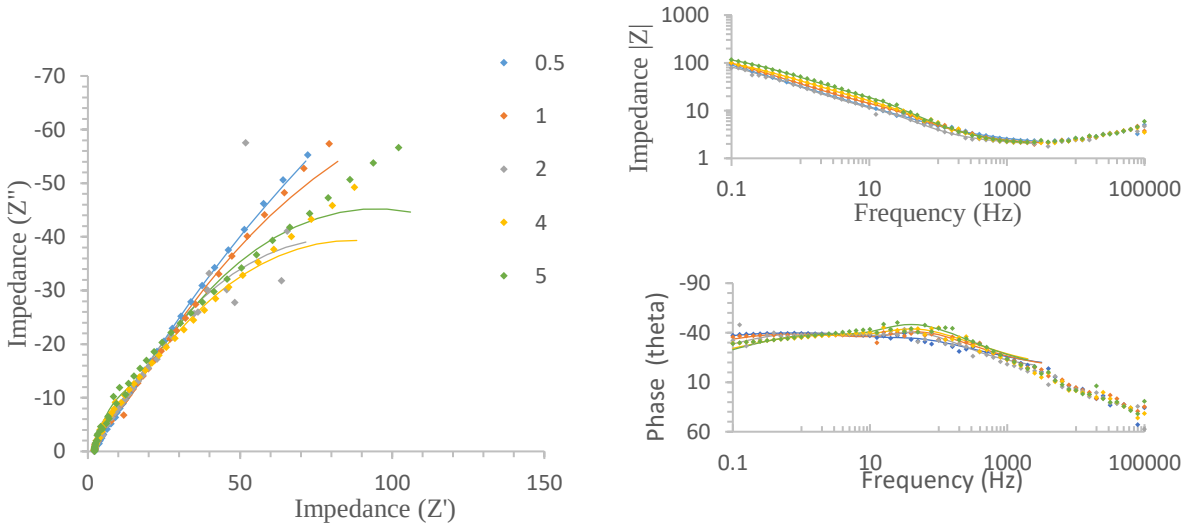

Figure 12. Nyquist (left) and Bode plots (right) for the immersion of SS304 in 700 °C FLiNaK for 4 hours.

In the case of SS304, the Rs remained constant, indicating consistent electrolyte conductivity. The double layer capacitance exhibited a decreasing trend, suggesting a reduction in the electrochemically active surface area due to corrosion processes. The charge transfer resistance increased gradually, indicating improved corrosion resistance with time. The constant phase element associated with the double layer capacitance showed a decreasing trend, potentially indicating changes in surface properties or adsorbed species during the corrosion process. Conversely, the CPE-P displayed an increasing trend, suggesting the formation or growth of a passive film on the alloy surface. The data for each component at each time interval is seen in Table 13.

Table 13. SS304 EIS data from Corrosion mechanism model.

Hrs	0.5	1	2	4	5
Chi-Sqr	0.001703	0.002156	0.004685	0.002928	0.002822
Sum-Sqr	0.14647	0.18541	0.39355	0.24011	0.23142
Rs(Ω)	1.847	1.814	1.873	1.682	1.799
Rs(Error)	0.058134	0.055807	0.071799	0.069643	0.064016
Rs(Error%)	3.1475	3.0765	3.8334	4.1405	3.5584
C(F)	0.00455	0.001598	0.002074	0.001951	0.001384
C(Error)	0.001174	0.000197	0.000377	0.000198	0.000151
C(Error%)	25.795	12.317	18.158	10.125	10.897
R(Ω)	0.97863	3.7	2.91	3.963	6.685
R(Error)	0.27734	0.37389	0.52489	0.56882	0.72081
R(Error%)	28.34	10.105	18.037	14.353	10.782
CPE-T($S \cdot s^n$)	0.012523	0.010434	0.010649	0.007818	0.006278
CPE-T(Error)	0.000356	0.000343	0.000522	0.000338	0.000279
CPE-T(Error%)	2.8457	3.2827	4.8987	4.3265	4.4372
CPE-P(°)	0.50563	0.55067	0.59845	0.57183	0.61339
CPE-P(Error)	0.009106	0.010096	0.018307	0.012243	0.011149
CPE-P(Error%)	1.8009	1.8334	3.0591	2.141	1.8176
Rp(Ω)	490.5	287.9	156.2	163.1	172.8
Rp(Error)	91.715	36.112	17.932	12.049	11.405
Rp(Error%)	18.698	12.543	11.48	7.3875	6.6001

4.4.2 Tafel

Figure 13 shows the potential vs log current tafel plot obtained during the immersion of SS304c. The first two scans, 0.5 and 1-hour, are seen to have similar E_{corr} values and slightly decrease with time. The 2-hour mark sits as an outlier in this graph, this is from external perturbation of the apparatus, as even a slight nudge to the system will require it to reach equilibrium again. Even though the 2-hour scan is an outlier, it was left in to show what even a small perturbation will do to the system, but any corrosion rate, Rp, or any other value calculated should not be considered when ranking structural materials, so the data in Table 14 will have a strikethrough on it for this reason. Looking at the 4 and 5-hour scans, the E_{corr} are lower than the 0.5 and 1-hour scans, showing that more corrosion is occurring than previous immersion. SEM would be a good technique here to determine any oxide layer formation and thickness on the surface of SS304 before immersion, and after approximately 1 hour of immersion, since SS304 oxide layers are generally prepared in the 700 °C range and could have survived the FLiNaK environment long enough to support the E_{corr} trend seen.

SS304c (Ni-8.09/Cr-18.23/Fe-72.32) exhibited a decreasing corrosion rate, from 1.36 to 0.69 mmpy, suggesting enhanced corrosion resistance over time. The corrosion rates are higher than the other nickel-based alloys, owing to the small amount of nickel, and high amount of chromium and iron seen in its composition. The corrosion rate was found to be 1.39 mmpy after 0.5 hours of immersion, slightly decreasing after 1 hour. After 4 hours of immersion the corrosion rate slightly decreased to 1.18 mmpy, then greatly decreased to 0.7 mmpy after 5 hours of immersion.

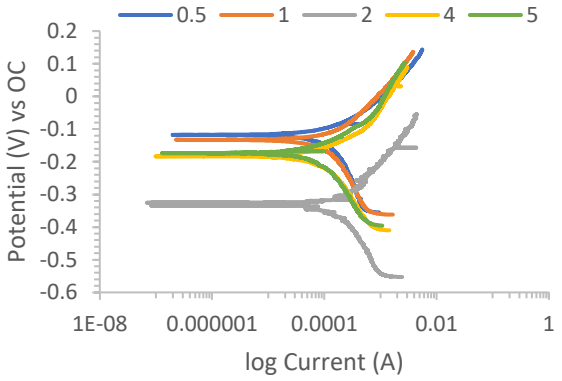

Figure 13.Tafel for SS304c. Density = 8.0 g/cm^3, area = 0.716 cm^2, EW = 24.69.

Table 14. Corrosion rates, corrosion potentials, corrosion currents, and beta constants for Stainless steel 304 in 700 °C FLiNaK salts.

Hrs	0.5	1	~~2~~	4	5
CR (mmpy)	1.39	1.29	~~2.72~~	1.18	0.70
E_{corr} (mV)	-121.57	-135.15	~~-334.64~~	-180.67	-170.22
I_{corr} (µA)	98.91	91.20	~~193.37~~	83.46	49.34
Cathodic Beta (mV)	135.52	124.79	~~186.45~~	195.74	148.99
Anodic Beta (mV)	90.19	115.83	~~138.58~~	122.65	68.19

4.4.3 Linear Polarization Resistance

Figure 14 shows the LPR data for the immersion of SS304c in 700 °C FLiNaK for 5 hours. The Rp remained fairly steady within the first hour of immersion, around 22 Ω. The 4th hour of immersion showed a high Rp value of 107, which is a big increase from the 1st hour of immersion. The 5th hour shows a decrease in Rp down to 78 Ω. Just as tafel, the 2-hour LPR scan shows a big deviation from the rest of the system due to an external perturbation on the apparatus and the 2-hour analysis has a strikethrough on Table 15, where the rest of the analysis values can be found. Tafel had shown E_{corr} lowering in the order of 0.5, 1, 5, and 4 hours but LPR shows 1, 0.5, 5, and 4 hours of E_{corr} decreasing. LPR is a very short scan, that spans 40 mV and at a scan rate of 1 mV/s, the technique takes 40 seconds. Since the previous perturbation in the system at the 2-hour mark occurred, it is likely that the Rp values obtained show the system is still not at equilibrium even after 2 hours but the tafel does not necessarily support this. A second experiment repeating everything would likely be needed in this scenario, sans external perturbation to the apparatus.

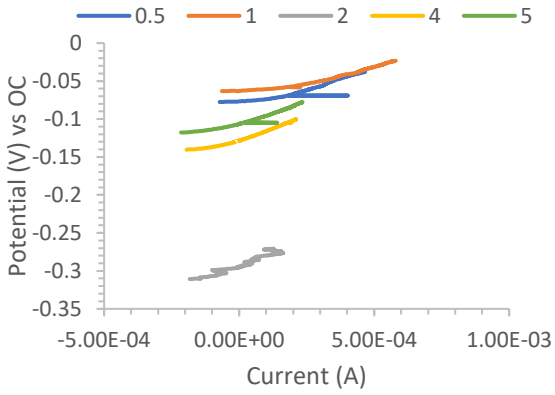

Figure 14. Linear polarization resistances for SS304c in 700 °C FLiNaK for 5 hours.

Table 15. Immersion time, polarization resistance, and normalized Rp values for SS304c in 700 °C FLiNaK over 5 hours.

Hrs	0.5	1	~~2~~	4	5
Rp	20.281	22.218	~~91.358~~	107.117	78.488
Ω-cm^2	14.52	15.90	~~65.39~~	76.66	56.17

4.5 Inconel 617 coupon

4.5.1 Electrochemical Impedance Spectroscopy

The Nyquist plot for Inconel 617 coupon (I617c) in Figure 15 shows both imaginary and real impedance increasing with time. An increase in the physical resistance from real impedance would suggest formation of a passivation later as time increases. An increase in the magnetic field capacity from imaginary impedance is also seen over time. The imaginary and real impedance of I617c increases as time increases, suggesting that an oxide layer might have been responsible for the lower impedance at the beginning of the experiment when the FLiNaK corroded it off and it then evolved a more stable fluoride passivation layer afterwards. The bode plots show that the magnitude of impedance vs frequency results in the same trend of impedance increasing over time in the low frequency range and then remaining the same and that it achieves a steady state in the higher.

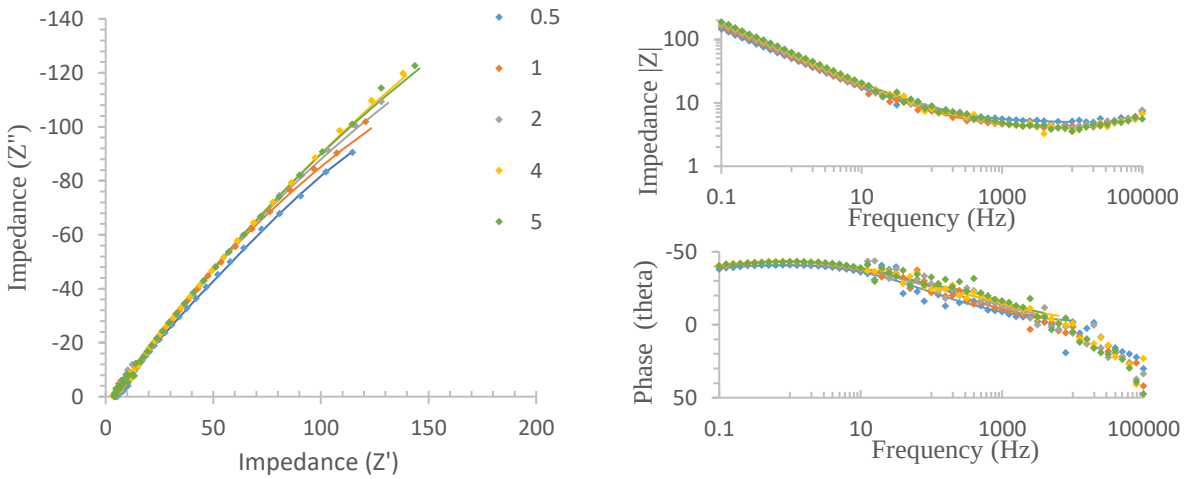

Figure 15. Nyquist (left) and Bode plots (right) for the immersion of I617 in 700 °C FLiNaK for 5 hours.

For Inconel 617, EIS revealed significant trends in the corrosion behavior and interfacial processes. The Rs displayed a decreasing trend, indicating enhanced electrolyte conductivity with time. The double layer capacitance exhibited a decreasing trend, suggesting potential changes in the electrochemically active surface area due to corrosion processes or formation of corrosion products. The charge transfer resistance also decreased, indicating improved corrosion resistance as the reaction progressed. The constant phase element associated with the double layer capacitance showed a decreasing trend, potentially indicating changes in the surface morphology or composition during the corrosion process. Conversely, the CPE-P remained relatively stable, suggesting the persistence of

the passive film during the immersion. The data for each component at each time interval is seen in Table 16.

Table 16. I617 EIS data from Corrosion mechanism model.

Hrs	0.5	1	2	4	5
Chi-Sqr	0.004131	0.002033	0.002055	0.002431	0.003037
Sum-Sqr	0.39658	0.17893	0.17672	0.22365	0.26724
Rs(Ω)	4.766	3.918	3.817	3.676	3.624
Rs(Error)	0.11657	0.092379	0.096422	0.090898	0.11186
Rs(Error%)	2.4459	2.3578	2.5261	2.4727	3.0866
C(F)	0.027889	0.002812	8.78E-04	7.40E-04	5.88E-04
C(Error)	1.69E-02	2.09E-03	3.90E-04	5.77E-04	2.18E-04
C(Error%)	60.619	74.401	44.414	77.942	37.091
R(Ω)	144	0.82792	0.81006	0.44999	0.95196
R(Error)	53.573	0.40335	0.30279	0.23228	0.34517
R(Error%)	37.203	48.718	37.379	51.619	36.259
CPE-T($S \cdot s^n$)	0.007121	0.006978	0.006624	0.006282	0.005966
CPE-T(Error)	0.000611	0.000218	0.000214	0.00021	0.000227
CPE-T(Error%)	8.5747	3.1263	3.235	3.3423	3.8101
CPE-P(°)	0.5513	0.56076	0.55118	0.53785	0.54656
CPE-P(Error)	0.017654	0.012554	0.012026	0.010795	0.013537
CPE-P(Error%)	3.2022	2.2387	2.1819	2.0071	2.4768
Rp(Ω)	179.5	655.3	820.4	1090	960
Rp(Error)	97.614	136.7	200.7	374.13	274.72
Rp(Error%)	54.381	20.861	24.464	34.324	28.617

4.5.2 Tafel

Figure 16 shows the tafel data for the immersion of I617c in 700 °C FLiNaK for 5 hours. Although the Nyquist plot showed impedance increasing, suggesting the resistance was going up, the tafel plot shows, from the 0.5 to the 5th hour immersion mark, the E_{corr} decreased. There are no passivation regions seen in the tafel plots anodic branch either. So, removing the possibility of a passivation layer suggests that real impedance increasing over time was due to specific components

of I617c corroding out first, then the alloy stabilizes as time goes on and experiences uniform corrosion of what elements are left.

The corrosion rate of Inconel 617 (Ni-52.7/Cr-22.29/Fe-2.17/Mo-0.3) remained relatively stable, from 0.54 to 0.57 mmpy, during the exposure, indicating consistent corrosion resistance throughout the testing period. Although the magnitude of the corrosion is higher than Inconel 600's, due to the decreased amount of nickel and increased amount of chromium, which is unstable in FLiNaK. The corrosion rate was found to be 0.54 mmpy after 0.5 hour of immersion, with a slight decrease to 0.46 mmpy after 1 hour. The corrosion rate remained steady after 2 hours of immersion, at 0.49 mmpy, and then increased from 0.52 and ending at 0.57 mmpy after 4 to 5 hours of immersion, respectively. Table 17 shows the β constants obtained from the tafel plot, then the use of equations 4 and 5 on the tafel plot to determine I_{corr} and CR's at each time interval.

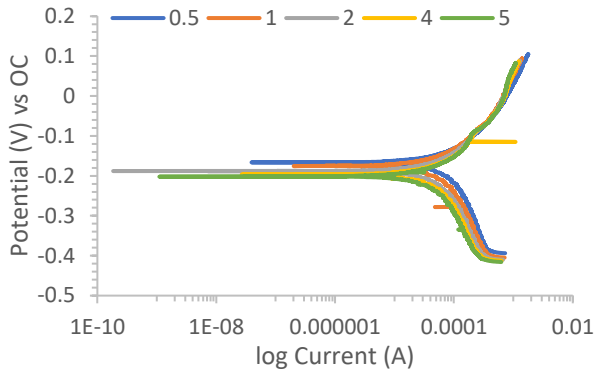

Figure 16.Tafel for I617. Density = 8.36 g/cm^3, area = 0.323 cm^2, EW = 14.93.

Table 17. Corrosion rates, corrosion potentials, corrosion currents, and beta constants for Inconel 617 coupon in 700 °C FLiNaK salts.

Hrs	0.5	1	2	4	5
CR (mmpy)	0.54	0.46	0.49	0.52	0.57
E_{corr} (mV)	-167.04	-169.23	-188.84	-193.54	-201.95
I_{corr} (µA)	29.97	25.64	26.98	28.97	31.52
Cathodic Beta(mV)	79.88	133.15	88.33	138.74	99.60
Anodic Beta(mV)	59.64	45.85	81.70	79.97	88.64

4.5.3 Linear Polarization Resistance

Figure 17 shows the LPR data for the immersion of I617 in 700 °C FLiNaK for 5 hours. The 0.5-hour scan showed the lowest E_{corr} value, followed by the 5th hour scan. The 1st, 2nd, and 4th hour scans show a trend of E_{corr} becoming more positive as time increases. The slope analysis of the LPR measurements showed the 0.5-hour scan to be the highest point, as time increases the polarization resistance reduces to single digit Ω-cm^2 values, then starts to increase again at the 5th hour scan. Two possibilities are that the 5th hour scan is either erroneous or a passivation layer started to form here. To further understand this, a longer immersion time could be used, or the sample could be analyzed further, for example by SEM, to see if any passivation layer was generated. The Rp and normalized Rp can be seen at each time interval in Table 18.

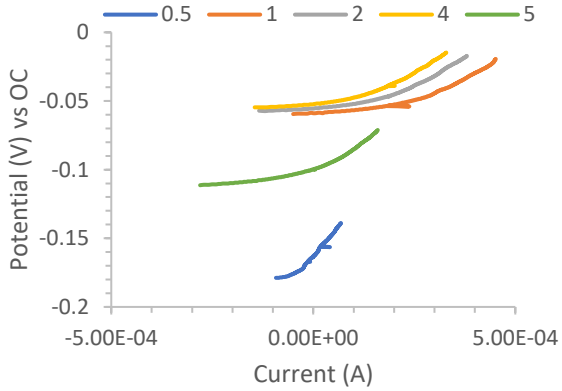

Figure 17. Linear polarization resistances for I617 in 700 °C FLiNaK for 5 hours.

Table 18. Immersion time, polarization resistance, and normalized Rp values for I617 in 700 °C FLiNaK over 5 hours.

Hrs	0.5	1	2	4	5
Rp	270.04	20.866	26.619	28.622	95.952
Ω-cm^2	87.34	6.74	8.60	9.25	31.03

4.6 Inconel 600 coupon

4.6.1 Electrochemical Impedance Spectroscopy

The Nyquist plot shows what appear to be two sets of data, the 0.5- and 1-hour set, then the 2,4, and 5-hour set. Between the 0.5- and 1-hour set, the imaginary and real impedance do not change. Then the imaginary and real impedance both increase and remains almost the same for the 2,4-, and 5-hour data. Observing the distance moved on the x-axis, the real impedance increased from 190 to 207 Ω, suggesting that the physical resistance of the system increased by 17 Ω. The y-axis, imaginary impedance, increases from -162 to -190, a difference of 28 Ω. The biggest increase is in the imaginary impedance, which represents the electric current stored in the electric field in the double layer. This would suggest that the double layer thickness is increasing in system, and it was seen to occur after the 1st hour of immersion. Since this was not seen on the I600w, this may be an artifact of inconel 600s geometry, which is planar here. The Bode plot supports the Nyquist plot findings, at a frequency of 0.1, the 0.5 and 1-hour immersion points are lower magnitude than the 2,4, and 5-hour immersion points. Then impedance slowly decreases until it reaches 1000 Hz, where it shows the electrolyte impedance.

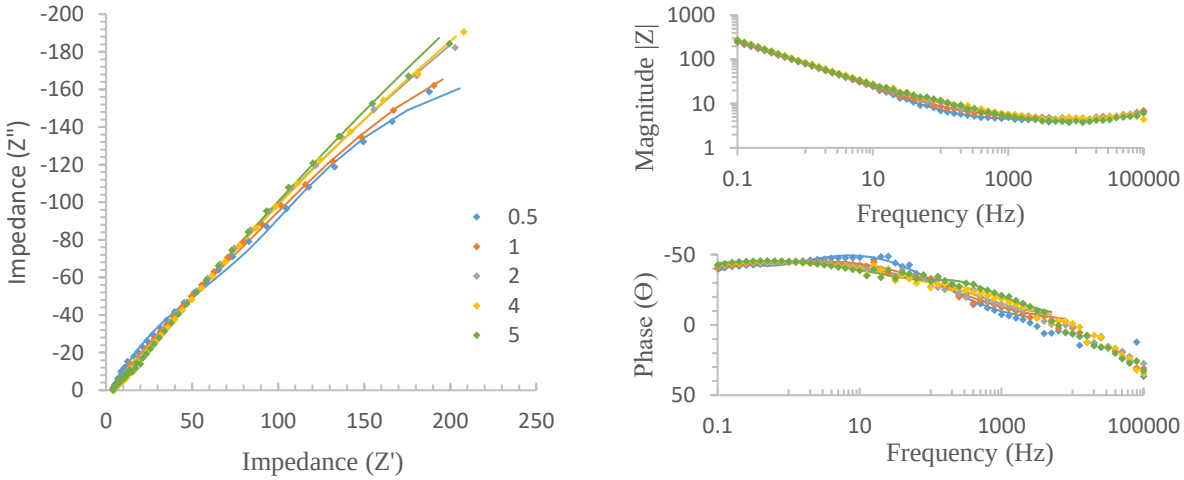

Figure 18. Nyquist (left) and Bode plots (right) for the immersion of I600c in 700 °C FLiNaK for 5 hours.

For the analysis of I600c, Rs remained unchanged, indicating consistent electrolyte conductivity. The double layer capacitance exhibited a decreasing trend, suggesting a reduction in the electrochemically active surface area, possibly due to corrosion products or passivation. The charge transfer resistance also decreased, indicating an improvement in corrosion resistance as the reaction

progressed. The constant phase element associated with the double layer capacitance showed a decreasing trend, suggesting changes in surface properties or adsorbed species during the corrosion process. Similarly, the CPE-P exhibited a decreasing trend, indicating the possible degradation or thinning of the passive film with time. Additionally, the polarization resistance increased, suggesting an enhancement in the material's resistance against corrosion. The data for each component at each time interval is seen in Table 19.

Table 19. I600c EIS data from Corrosion mechanism model.

Hrs	0.5	1	2	4	5
Chi-Sqr	0.000916	0.000945	0.001068	0.001305	0.00091458
Sum-Sqr	0.076954	0.088814	0.096144	0.11746	0.082313
Rs(Ω)	4.089	4.232	4.313	4.07	3.588
Rs(Error)	0.049784	0.052586	0.079181	0.087509	0.068593
Rs(Error%)	1.2175	1.2426	1.8359	2.1501	1.9117
C(F)	0.00765	0.011057	1.70E-03	3.96E-04	3.70E-04
C(Error)	0.000426	1.66E-03	1.05E-03	8.53E-05	4.26E-05
C(Error%)	5.5717	15.011	61.496	21.551	11.531
R(Ω)	303.2	291.3	0.53889	1.533	2.679
R(Error)	17.483	28.559	0.31263	0.31007	0.2934
R(Error%)	5.7662	9.804	58.014	20.226	10.952
CPE-T($S \cdot s^n$)	0.002639	0.003984	0.004363	0.004315	0.0045497
CPE-T(Error)	8.49E-05	1.32E-04	9.24E-05	1.02E-04	8.83E-05
CPE-T(Error%)	3.2167	3.315	2.1167	2.3734	1.9404
CPE-P(°)	0.69667	0.59029	0.54959	0.54289	0.546
CPE-P(Error)	0.006763	0.006636	0.007696	0.008339	0.0070976
CPE-P(Error%)	0.97069	1.1242	1.4003	1.5361	1.2999
Rp(Ω)	119	211.4	1888	2237	2.79E+03
Rp(Error)	6.9819	34.2	422.54	639.55	9.01E+02
Rp(Error%)	5.8671	16.178	22.38	28.59	32.322

4.6.2 Tafel

Figure 19 shows the potential vs log current Tafel plot obtained during I600c immersion in 700 °C FLiNaK salts for 5 hours. The E_{corr} hovers around the -0.2 V area for the duration of the experiment, suggesting corrosion occurred but the potential did not change. The I600w tafel does not show the same trend, which showed E_{corr} becoming more positive over time, but the 4th hour points do support each other very well. The 4th hour E_{corr} for I600w was -0.18 while the 4th hour E_{corr} for I600c was -0.20, only a 20 mV difference, a smaller range than the LPR scan. Which may say the I600w early immersion time took longer to stabilize. The anodic branches are all similar except for the 0.5-hour study. The 0.5-hour scans are usually obtained before the system can reach a steady state temperature, so the 0.5-hour scan is not too indicative of an analytical value. The E_{corr}, I_{corr}, tafel constants, and corrosion rates can all be seen in Table 20.

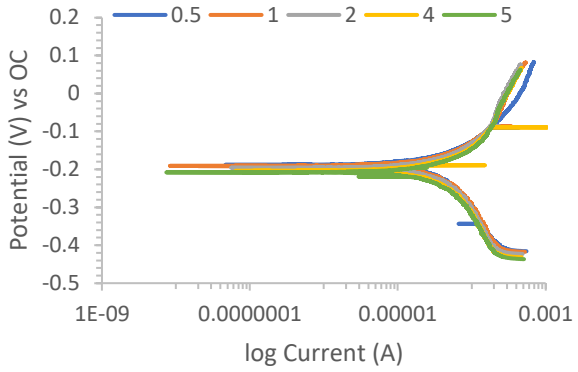

Figure 19.Tafel for I600c. Density = 8.47 g/cm^3, area = 0.311 cm^2, EW = 24.83.

Table 20. Corrosion rates, corrosion potentials, corrosion currents, and beta constants for Inconel 600 coupon in 700 °C FLiNaK salts.

Hrs	0.5	1	2	4	5
CR (mmpy)	0.44	0.62	1.12	0.76	1.04
E_{corr} (mv)	-184.05	-190.52	-198.37	-206.12	-209.27
I_{corr} (µA)	14.40	20.03	36.25	32.61	33.87
Cathodic Beta(mv)	92.42	103.79	138.65	150.16	182.63
Anodic Beta(mv)	44.88	81.57	173.91	128.89	115.42

4.6.3 Linear Polarization Resistance

Figure 20 shows the LPR data for I600c immersed in 700 °C FLiNaK for 5 hours. The potential vs current graph here shows no real trend for E_{corr} vs time. The 0.5 and 1-hour immersion points are very close, the 2 and 4-hour immersion points are also close, then the 5th hour mark for LPR shows a very low E_{corr}. This trend isn't supported by tafel or EIS. The normalized Rp values do not show a trend either, which is not supported by the I600w data either. The Rp and normalized Rp can be seen at each time interval in Table 21.

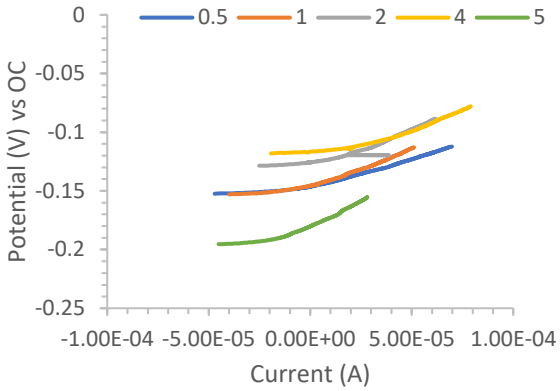

Figure 20. Linear polarization resistances for I600w in 700 °C FLiNaK for 5 hours.

Table 21. Immersion time, polarization resistance, and normalized Rp values for I600w in 700 °C FLiNaK over 5 hours.

Hrs	0.5	1	2	4	5
Rp	339.444	432.709	226.886	149.851	702.427
Ω-cm^2	105.55	134.55	70.55	46.59	218.42

4.7 HastelloyN coupon

4.7.1 Electrochemical Impedance Spectroscopy

Figure 21 shows very little change in impedance over time. From 0.5 hours of immersion to 2 hours, the impedance value was 270 Ω, which at the 4- and 5-hour mark jumped up to 300 Ω of impedance. The impedance values correspond to a resistance to being polarized, which is a highly sought after property for storage materials. The bode plots for HastelloyN, which support the Nyquist plot conclusion of very little change in impedance over the 5 hours of immersion. The |Z| vs Hz bode plot shows that as frequency increases the impedance decreases. The 0.1 Hz range will show the impedance of the whole system being 364 Ω. The steady state impedance values beyond 1,000 Hz show electrolyte impedance to be around 11 Ω and therefore HastelloyNs impedance as 353 Ω.

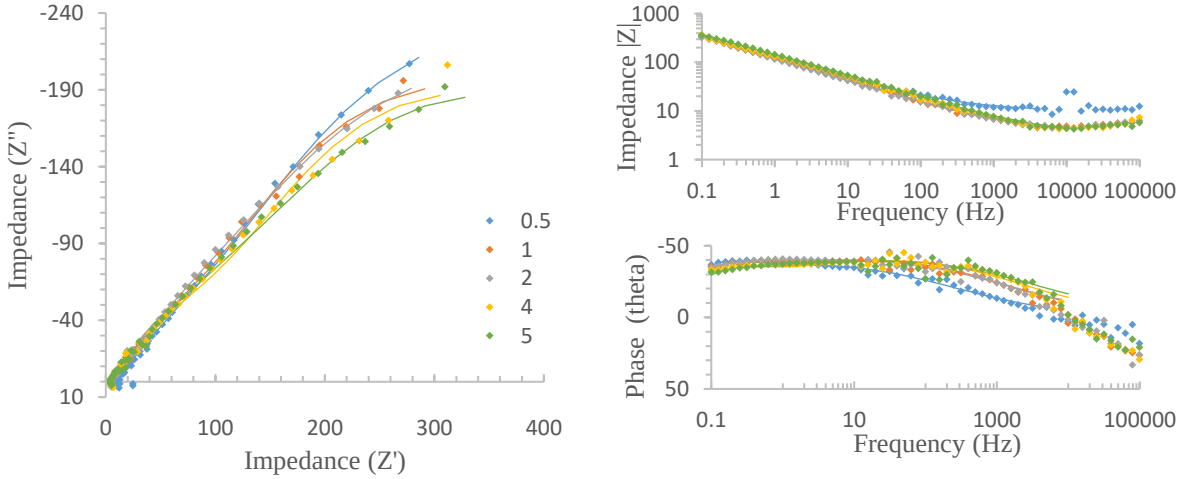

Figure 21. Nyquist (left) and Bode plots (right) for the immersion of HastelloyN in 700 °C FLiNaK for 5 hours.

The EIS for HastelloyN showed the Rs displayed a decreasing trend, indicating improved electrolyte conductivity. The double layer capacitance showed an increasing trend, suggesting potential changes in the electrochemically active surface area, possibly due to the formation of corrosion products or passivation. The charge transfer resistance decreased, indicating improved corrosion resistance as the reaction progressed. Interestingly, the constant phase element associated with the double layer capacitance and the CPE-P remained relatively stable, indicating the preservation of surface characteristics and the stability of the passive film during immersion. Additionally, the polarization resistance also remained unchanged, suggesting a consistent level of resistance against corrosion. The observed variations in the equivalent circuit parameters provide

insights into the evolving interfacial processes and corrosion mechanisms of Hastelloy N. The data for each component at each time interval is seen in Table 22.

Table 22. HastelloyN EIS data from Corrosion mechanism model.

Hrs	0.5	1	2	4	5
Chi-Sqr	0.002051	0.002183	0.002788	0.002892	0.0039981
Sum-Sqr	0.18049	0.20515	0.26208	0.27767	0.38382
Rs(Ω)	9.554	3.695	3.543	3.273	2.996
Rs(Error)	0.29263	0.1252	0.14091	0.13445	0.17463
Rs(Error%)	3.0629	3.3884	3.9771	4.1079	5.8288
C(F)	8.02E-03	6.52E-03	1.10E-02	6.30E-03	0.0080093
C(Error)	1.80E-03	9.05E-04	1.85E-03	7.77E-04	0.002154
C(Error%)	22.443	13.881	16.799	12.325	26.894
R(Ω)	332	303.1	230.8	300.7	239.1
R(Error)	50.159	27.991	40.461	29.208	44.65
R(Error%)	15.108	9.2349	17.531	9.7133	18.674
CPE-T($S \cdot s^n$)	0.002894	0.002442	0.002976	0.002006	0.0021313
CPE-T(Error)	0.000243	0.000151	0.000189	0.000128	0.00016326
CPE-T(Error%)	8.3897	6.1847	6.3605	6.3635	7.6601
CPE-P(°)	0.50206	0.53067	0.50598	0.52996	0.50592
CPE-P(Error)	0.014891	0.009917	0.011288	0.010244	0.012015
CPE-P(Error%)	2.966	1.8688	2.2309	1.933	2.3749
Rp(Ω)	320.8	232.5	415.7	231.4	349.4
Rp(Error)	91.369	35.018	71.563	26.177	75.442
Rp(Error%)	28.482	15.062	17.215	11.312	21.592

4.7.2 Tafel

Figure 22 shows the potential vs log current tafel plot obtained during HastelloyN immersion in 700 °C FLiNaK salts for 5 hours. The E_{corr} shows a clear trend from the 0.5-hour immersion mark to the 5th hour mark that E_{corr} is decreasing with time. The anodic branches show very typical and linear tafel regions with no significant deviations, such as passivation zones. The cathodic branches show a trend of decreasing current over time, which could suggest that contamination from the first hour of corrosion has diffused away from the working electrode.

HastelloyN (Ni-69.27/Cr-7/Fe-4/Mo-16/Co-0.02) demonstrated a decreasing corrosion rate, suggesting effective corrosion resistance and the beneficial influence of its composition, particularly the presence of molybdenum and nickel. The corrosion rates were seen to start at 0.52 mmpy but decrease over time and was calculated to be 0.36 mmpy at the 5th hour scan. The E_{corr}, I_{corr}, tafel constants, and corrosion rates can all be seen in Table 23.

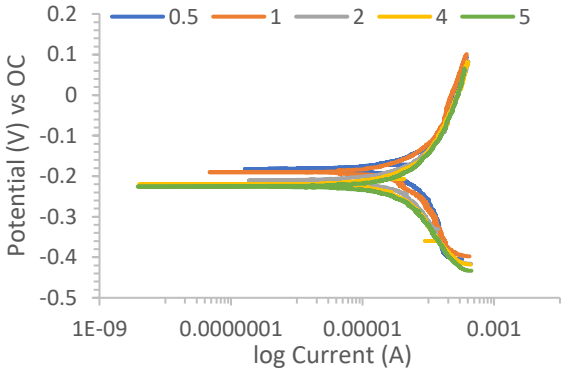

Figure 22. Tafel for HastelloyN. Density 8.86 g/cm^3, area = 0.469 cm^2, EW = 27.22.

Table 23. Corrosion rates, corrosion potentials, corrosion currents, and beta constants for HastelloyN in 700 °C FLiNaK salts.

Hrs	0.5	1	2	4	5
CR (mmpy)	0.52	0.48	0.41	0.47	0.36
E_{corr} (mV)	-182.29	-187.80	-212.36	-222.31	-224.35
I_{corr} (µA)	24.38	22.19	19.36	21.97	16.93
Cathodic Beta (mV)	105.16	85.79	77.61	75.48	85.75
Anodic Beta (mV)	88.42	99.84	109.84	157.01	77.31

4.7.3 Linear Polarization Resistance

Figure 23 shows the LPR data for HastelloyN immersed in 700 °C FLiNaK for 5 hours. Aside from the 0.5-hour immersion mark, which typically deviates from trends seen, there is a trend that E_{corr} is decreasing with time for the 1st to 5th hour immersion scans. The slope analysis showed that polarization, from the 1st to 5th hour immersion scans, increased from 108 to 188 Ω-cm^2. The Rp and normalized Rp can be seen at each time interval in Table 24.

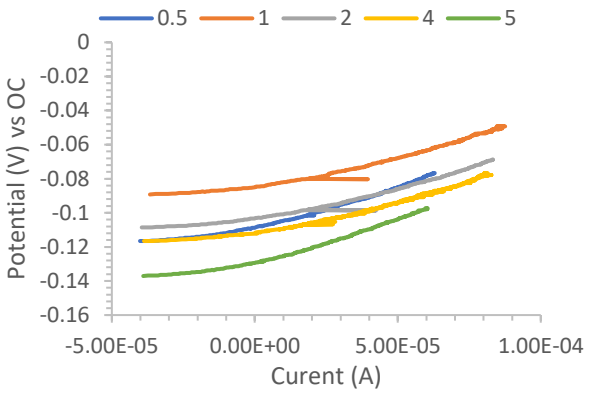

Figure 23. Linear polarization resistances for HastelloyN in 700 °C FLiNaK for 5 hours.

Table 24. Immersion time, polarization resistance, and normalized Rp values for HastelloyN in 700 °C FLiNaK over 5 hours.

Hrs	0.5	1	2	4	5
Rp	487.726	231.345	213.527	262.398	401.953
Ω-cm^2	228.53	108.40	100.05	122.95	188.34

4.8 EIS Equivalent Circuit Model

The Nyquist and Bode plots were all fit utilizing the equivalent circuit model seen in Figure 3. The equivalent circuit model has 5 main components, with 3 sections visible that are in series to each other. Starting from left to right, the Rs model is a resistor, and it represents the resistance associated with the electrolyte solution, which is also causing the corrosion of the structural materials. The Rs represents the FLiNaK salt at 700 °C, the environment responsible for corrosion. It is related to the ionic conductivity of the solution and affects the overall impedance of the system. By monitoring the changes in Rs, one can gain insights into the ionic transport properties and the presence of any solution-related limitations in the electrochemical system.

The second set of components is the C-R, which represents a capacitor in parallel with another resistor. The parallel components both represent the behavior associated with the double-layer capacitance, which includes any additional capacitance that is seen and observed in the system. The capacitor by itself purely represents double-layer capacitance, which is from the double layer formed at the electrode-electrolyte interface, that every working electrode experiences once immersed into an electrolyte. The R represents another resistor, which here models the resistance seen from passivation layers and corrosion products that inevitably diffuse out into the system. The last set of components are the CPE-Rp, this combination represents the interfacial processes at the electrode-electrolyte interface. The CPE element can model the double-layer capacitance for the working electrodes and is able to consider non-ideal behavior, which the system greatly exhibits. The Rp component is another resistor, which models the charge transfer resistance associated with the corrosion reaction kinetics at the interface.

Nickel EIS modeling showed chi-squared values ranging from 0.003 to 0.005 and sum of squared error values ranging from 0.31 to 0.53 in data taken over a 4-hour period. The Inconel 600 wire EIS model showed chi-squared values from 0.003 to 0.004 and sum of square values ranging from 0.28 to 0.39 over a 4-hour period. SS308 wire EIS modeling showed chi-squared error values ranging from 0.002 to 0.004 and sum of squared error values from 0.21 to 0.37 over a 4-hour period. SS304 EIS modeling showed chi-squared error values ranging from 0.002 to 0.004 and sum of squared error values ranging from 0.15 to 0.24 in data taken over a duration of 5 hours. HastelloyN EIS modeling showed chi-squared error values ranging from 0.002 to 0.004 and sum of squared error values ranging from 0.18 to 0.38. Inconel 617 EIS modeling showed chi-squared error values ranging from 0.002 to 0.004 and sum of squared error values ranging from 0.18 to 0.40. Inconel 600 EIS modeling showed chi-squared error values ranging from 0.0009 to 0.001 and sum of squared error values ranging from 0.09 to 0.11.

4.9 Ranking of materials

4.9.1 EIS impedance ranking

All the materials here are ranked according to the values determined at the 4-hour immersion mark by the max magnitude of impedance multiplied by the corrosion area that each working electrode experienced. Figure 24 shows nickel having the highest impedance at the 4-hour mark in 700 °C FLiNaK. The ranking for all the materials, from biggest to smallest, is nickel > I600w > HastelloyN > SS308 > I600c > SS304 > I617, where higher impedance is better. As mentioned previously, nickel fluoride passivation starts very early and is established within 4 hours in FLiNaK at 700 °C. The two following materials, inconel and HastelloyN, have been shown to have the highest nickel content out of the rest of the materials which pushes them ahead, in terms of impedance.

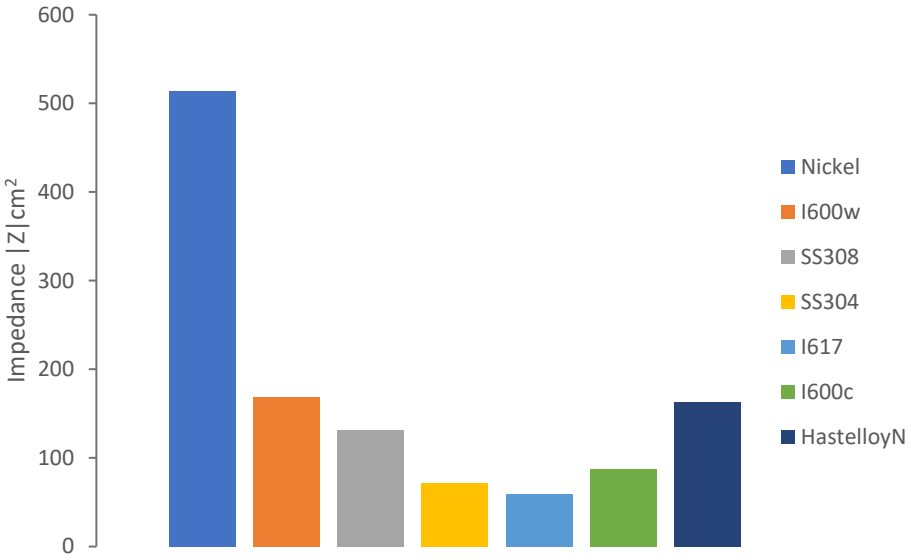

Figure 24. Normalized impedance of all materials at the 4th hour of immersion in 700 °C FLiNaK. The ‘w’ represents a wire, and the ‘c’ represents a coupon for the legend.

4.9.2 Corrosion rate rankings

Figure 25 shows the corrosion rate at the 4th hour of immersion for each material tested in 700 °C FLiNaK. The nickel sample showed the lowest corrosion rate out of the entire set, which it was theorized to do and demonstrated experimentally it would. The ranking of corrosion rates, from smallest to biggest, is nickel < HastelloyN < Inconel 600 < Inconel 617 < SS304 < SS308, where smaller corrosion rate is better. HastelloyN and Inconel 600 have the highest nickel concentrations of this series of alloys, which would explain the lower corrosion rates than I617 and SS304.

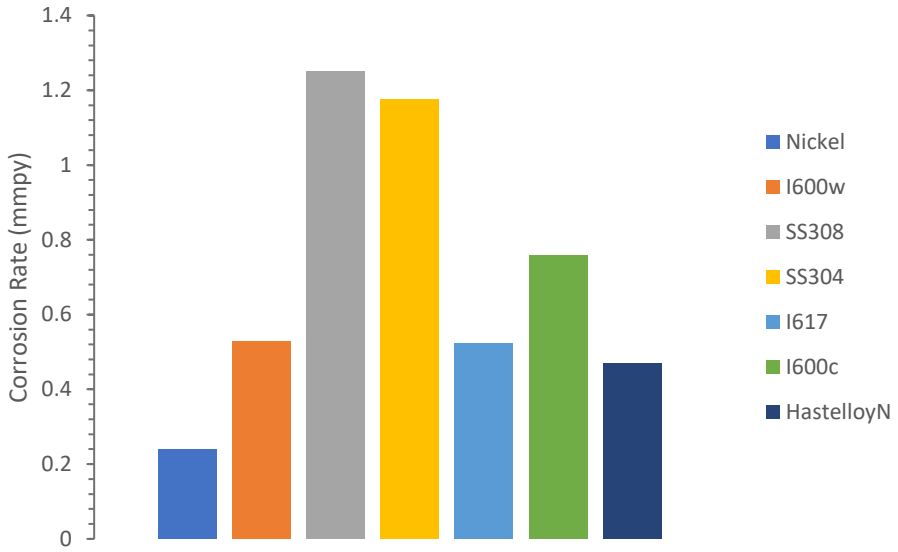

Figure 25. Ranking of structural materials in 700 °C FLiNaK salt in 4 hours. The 'w' represents a wire, and the 'c' represents a coupon for the legend.

The corrosion rates are capable of being compared to other tested alloys results[23,42] in FLiNaK salts at temperatures in the 680 – 700 °C range, which closely relates or exactly matches the temperature used in this study, 700 °C with result examples in Table 25. The results of other studies showed high nickel-based alloys also exhibited corrosion rates in the ~0.50 mmpy region. Assuming contamination of H_2O and O_2 are below 5 ppm, the results are directly comparable.

Table 25. Similar alloy tests in FLiNaK at similar temperatures assisting in the decision of picking a tafel analysis method.

Material	Temp (C)	CR (mmpy)
Nimonic 80A	680	0.50
Inconel 718	680	0.45
Inconel C-276	680	0.05
Inconel 600	700	0.645
Inconel 617	700	0.861
Inconel 625	700	1.811

4.9.3 LPR rankings

Figure 26 shows the normalized polarization resistances found at the 4th hour of immersion in 700 °C FLiNaK for each material tested. As with EIS, nickel is shown to have the highest Rp amongst the entire set of materials. It was seen in the results section that after 2 hours, nickel forms a passivation layer of fluorides and becomes very stable in FLiNaK. The ranking for the materials, from biggest to smallest, is nickel > I600w > HastelloyN > SS304 > I600c > SS308 > I617, where higher Rp is better. I600 and HastelloyN are 2nd and 3rd in the ranking after nickel, again, due to their high nickel compositions, which are 72% and 70% respectively. I617 and SS308 come in last place not just due to the lack of nickel, but due to the high chromium composition, which are 22.3% and 20.5% respectively, which is the least stable alloy material in FLiNaK.

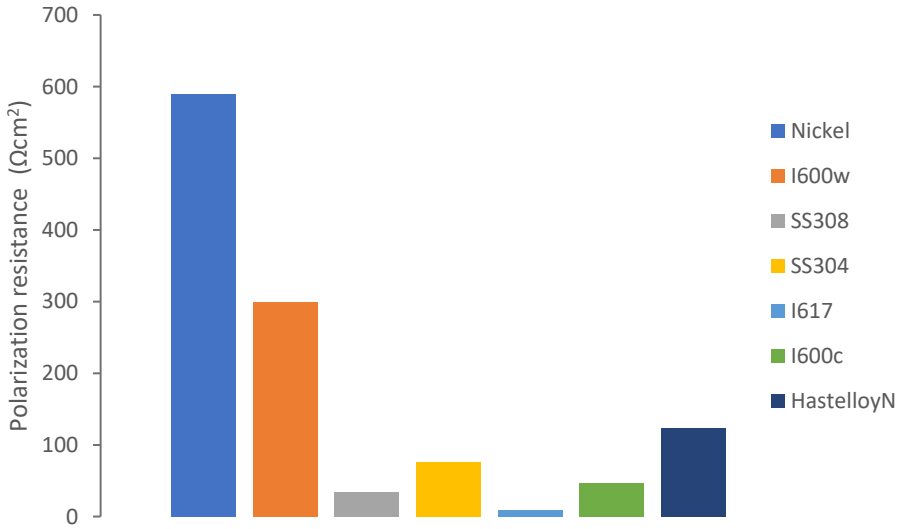

Figure 26. Normalized polarization resistance of all materials in 700 °C FLiNaK at the 4th hour of immersion. The ‘w’ represents a wire, and the ‘c’ represents a coupon for the legend.

Chapter 5: Conclusion

In conclusion, this study aimed to rank materials based on their performance in 700 °C FLiNaK by evaluating corrosion rates, polarization resistances, and impedance characteristics. These factors collectively contribute to the overall ranking determination with lower corrosion rates, higher polarization resistances, and stable impedance profiles indicating the best material performance. It was found that nickel was the most stable in FLiNaK at 700 °C after 4 hours of immersion, which suggests that it would be a suitable material for use in nuclear reactors if it could be electrochemically plated onto other structural materials that provide structural stability, which it lacks. Otherwise, Inconel 600 or HastelloyN were the best ranked structural materials. Additionally, an equivalent circuit model was fit to all the impedance data collected from all the materials tested, which provides a framework for understanding the behavior of materials in FLiNaK, such as polarization resistances, ion transport, interfacial reactions, and the formation of passive layers.

These results have significant implications for the design and operation of next-generation nuclear reactors, as they highlight the importance of material selection and provide insights into the mechanisms that govern material performance in extreme environments. Overall, this study represents a valuable contribution to the field of nuclear materials science and underscores the need for continued research in this area by providing insights into the corrosion behavior of structural materials in molten fluoride eutectic salts. The findings elucidate the corrosion mechanisms governing material performance, including the formation of passivation layers, the influence of composition on corrosion rates, and the impedance characteristics in 700 °C FLiNaK environments. These insights have direct implications for the design and selection of materials for next-generation nuclear reactors and other high-temperature applications involving molten salts, contributing to enhanced reliability, safety, and efficiency.

Future work from this study includes more experiments that focus on repeating the same tests to provide a statistical analysis of the data. Testing other alloys with high nickel or molybdenum content. Repeat testing at the 500 °C temperature range. Include classical immersion tests that span 100+ hours and compare this to the 4–5-hour immersion tests. Determine if instantaneous electrochemical corrosion testing can replace long duration tests and what time scale of immersion the electrochemical tests need to move to, e.g., will 5 hours of immersion with electrochemical tests be able to replace the 100+ hour testing, or how long will electrochemical immersion testing need to be to replace long term tests.

Appendix

A.1 Cylindrical vs Planar Electrodes

This analysis was performed because the testing materials received had changed from wires to coupons. Since experiments for I600 utilized cylindrical electrodes for the working electrodes and were later received in coupon form as well, a comparison was done. As the transport of charge and electrochemical products changes based on electrode geometry a comparison of planar vs cylindrical electrodes from electrochemical testing is shown.

Figure 27 is the EIS Nyquist plot at the 4th hour of immersion for both cylindrical I600w and planar I600c. The blue square represents the planar I600c electrode, and the gray circles represent the I600w cylindrical electrode. The data points, while not exact, match up with each other to show similar trends. Some differences can be seen from around the 100 Z′ portion of the graph but the differences in those values are not enough to warrant a new equivalent circuit model, as the Voigt model still fits both with less than 1 chi-sqr and approx. 1 sum of square values.

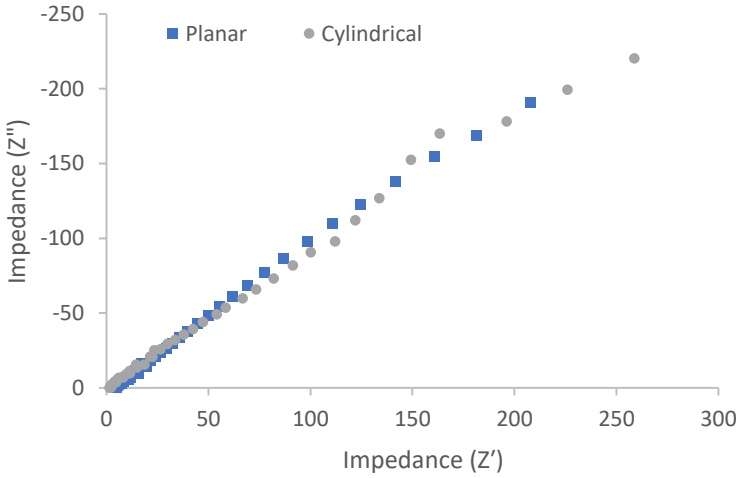

Figure 27. EIS analysis Nyquist plot showing the difference in impedance values obtained for cylindrical and planar electrodes both made of I600, each tested in 700 °C eutectic FLiNaK salt.

Figure 28 is the corrosion rates vs time for both inconel 600 geometries. Both samples show a similar trend of seeing corrosion rates from the 0.5 to 1 hour mark decrease and both samples show corrosion rates generally stabilizing at the 2nd hour mark and remaining the same to the 4th hour mark. The major difference seen is the actual values of the calculated corrosion rates. The 4th hour of immersion for the cylindrical sample returned a calculated corrosion rate of 1.2 mmpy and the planar sample was 2.5 mmpy, which is more than double the corrosion rate of the cylindrical sample. Additional testing could be done to try and add some statistical analysis to this approach, as it is

possible one, or both, of these samples could be an outlier, making it hard to distinguish between theory and experiment.

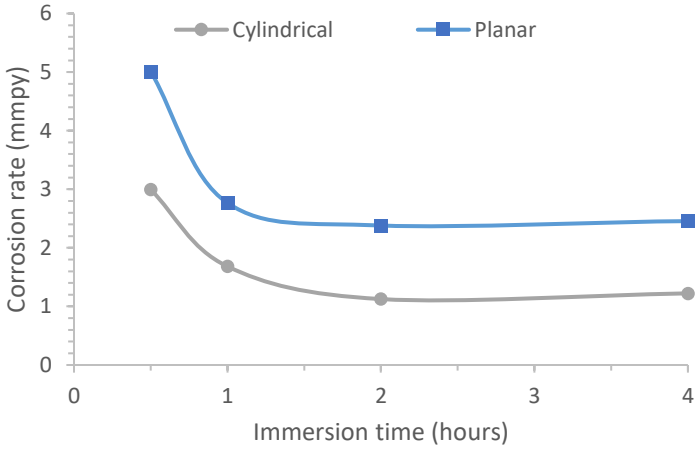

Figure 28. Tafel analysis showing the difference in CR values obtained for cylindrical and planar electrodes made of I600, both testing in 700 °C eutectic FLiNaK salts

Figure 29 shows the normalized Rp vs time for both inconel geometries. Aside from the 1st hour scan for the cylindrical sample, there appears to be an increase in Rp over time, suggesting a passivation layer began forming somewhere after the 2nd hour. The planar sample shows the opposite trend, which is a decreasing Rp over time. There is also a difference of approximately 200 Ω-cm^2 between both of the samples at each time interval. As mentioned for the previous tafel section, and even more deserving would be LPR analysis, is that the tests should be repeated to get statistically relevant data, in the event one, or both, of these experiments were outliers.

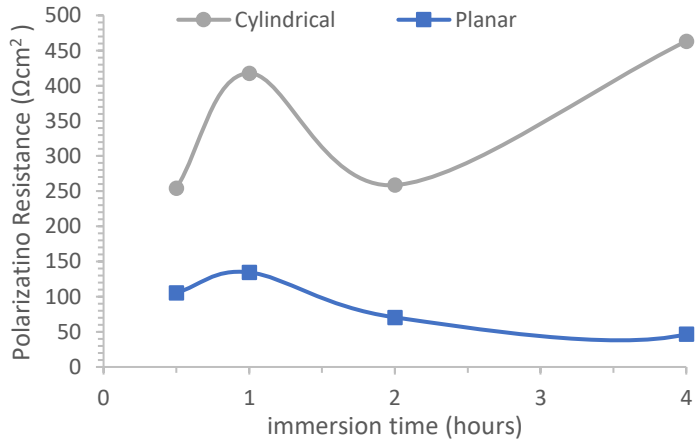

Figure 29. LPR analysis showing the difference in Rp values obtained for cylindrical and planar electrodes made of I600, both tested in 700 °C eutectic FLiNaK salt.

The conclusion for this section is that EIS showed very little differences between utilizing a planar electrode (coupon) or a cylindrical electrode (wire) when performing corrosion studies. Tafel showed a corrosion rate difference at least twice as high, and LPR showed approximately 200 Ω-cm^2 of difference between the two geometries. Comparing those two techniques will require some repeated experiments to gain a statistical understanding of how switching from planar to coupon may affect CR and Rp data. Theoretically it should not, and statistics may help prove that in this case.

A.2 Comparing Tafel Methods

The tafel method presented in the results section deviates from the tafel zones discussed in the ASM 13A guide. The method, which was utilized by Mansfeld[26], involved moving the analysis region close to E_{corr}, called Method 1, and can be seen in Figure 30 as M1. Seeking out a new method arose from corrosion rate calculations being 3 to 5 times higher values when compared to other journal articles. Another way of analyzing tafel, Method 2, is from others who also have shown problems with utilizing the cathodic branch data to determine corrosion rates in molten salt electrolytes[27-30]. Due to the lack of electrochemical reductions happening in the system, the cathodic branch extrapolation leads to offsets for corrosion rates. Method 2 involves solely utilizing the extrapolation of the anodic branch to determine i_{corr}. E_{corr} is determined from the tafel plot as the point where both branches come together to create a point. Example of tafel regions utilized can be seen in Figure 30 as M2.

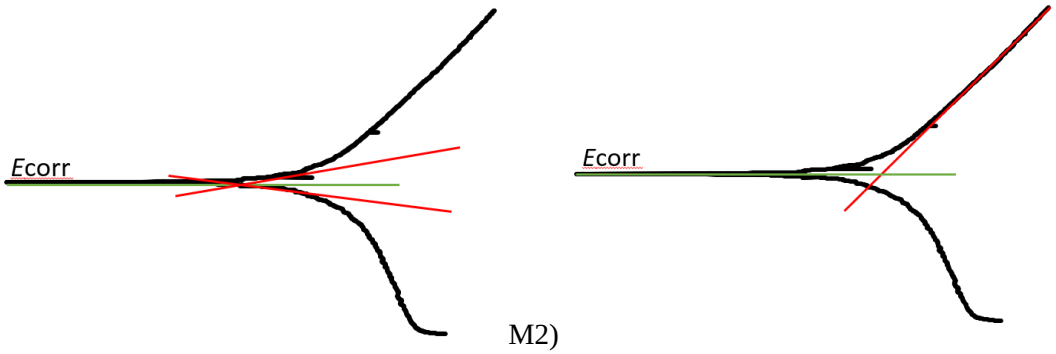

M1) M2)

Figure 30. 1) shows Method 1 for Tafel analysis and 2) shows Method 2 for Tafel analysis.

Method 1 was found to be the better method to use and was used during tafel analysis for the results section due to the results being comparable to other tested alloys results[23,42] in FLiNaK salts at temperatures in the 680 – 700 °C range, which closely relates or exactly matches the temperature used in this study, 700 °C with result examples in Table 25.

A.3 Voigt Finite Diffusion Model for Diffusion Coefficients

The Nyquist plots for all materials analyzed have exhibited a characteristic lone 45° angle, which is known as a mass diffusion-controlled system. If a semi-circle with a 45° after it is present, then the semi-circle region is known as kinetic-controlled region and the angle is known as the diffusion-controlled region. The diffusion-controlled region can be better understood by a model known as a Voigt equivalent circuit model[30]. Impedance studies[30-32] have shown that when using EIS to measure diffusion-limited systems, the Voigt circuit has been good to use for studying the error structure of experimental EIS data as well as modeling the system. The Voigt circuit was also proven that it satisfies the Kramers-Kronig relation[33.34], which is mathematically concerned with connecting both parts of the complex graph, i.e., Nyquist plots and the imaginary vs real values. Mathematical models of the Voigt model were also shown to be forced into a system by continually adding resistance-capacitance (RC) circuits to a similar system and obtained well-fitting results[35,36]. Further research on experimentally fitting the Voigt circuit to diffusion-controlled systems with a rotating disk electrode was performed to show how a kinetically driven system still fits into the Voigt model[37,38].

Figure 31 shows the equivalent circuit model also used to fit the data for the alloys. Starting left to right, Rs is a resistor component that was used to represent the resistance of the solution, also known as the electrolyte. The value for Rs is obtained from Nyquist plots where the x-intercept is located, the point where imaginary impedance is zero in the high frequency region, it is important to distinguish which frequency region since Nyquist plots can create a full semi-circle plot where the imaginary impedance is zero again at higher impedance values.

In series to the Rs component is a set of parallel components, C and Ws. C here is a general capacitor model and signifies the capability of the working electrode, the corroding alloy in this case, and its ability to perform as a capacitor. The impedance to capacitance relationship is given by:

$$Z = \frac{1}{j\omega C} \quad [39]$$

where Z is the impedance, *j* is the imaginary number, ω is the frequency, and C is the capacitance. The real impedance here is equal to 0 and the imaginary impedance is given by the following equation:

$$Z'' = \frac{-1}{\omega C} \quad [40]$$

Parallel to the capacitor is the finite length Warburg-short circuit terminus component (Ws). The Ws component, during modeling, has three parameters, labeled the Ws-R, Ws-T, Ws-P. The Ws-R parameter is used to describe resistance; Ws-T is used for diffusion interpretation and is given by the following relation:

$$Ws - T = \frac{L^2}{D} \quad [41]$$

where L is the effective diffusion thickness and the diffusion coefficient is given by D. Ws-P refers to the Warburg-shorts behavior to act either as a capacitor or a resistor, just as the CPE-P, where it varies between 0 to 1. Often the Ws-P is fixed to 0.5 but it was left as a free variable during the modeling process, which produced values with smaller errors. Impedance and the Ws component, with its parameters, are all equated to each other in the following equation:

$$Z = R\frac{\tanh[(jT\omega)^P]}{(jT\omega)^P} \quad [42]$$

where R is the Ws-R parameter, *j* is imaginary number, T is the Ws-T parameter, ω refers to frequency, and P is the Ws-P parameter. Because the Ws component is meant to model finite-length diffusion, logically it fits this system as the Nyquist plots for all alloys have shown complete diffusion-controlled behavior due to the lack of a kinetic controlled semicircle appearance.

The last set of components are the CPE-Rp, which are parallel with each other. The CPE component refers to a constant phase element, which is often used instead of a capacitor—hence the bent capacitor symbol in the circuit—to model non-homogeneity occurring in the system[36]. Non-homogeneity occurs when the surface of the alloy loses its perfection and becomes porous through general polarization and metastable pitting. The CPE is broken up into two parameters, T and P. The CPE-P refers to a component that varies between a capacitor or a resistor. The closer the CPE-P is to 1, the closer it is to a capacitor; the closer CPE-P is to 0, the closer it is to a resistor. The CPE-T parameter refers to a time constant that accompanies all capacitor components. The CPE component is governed by the following equation:

$$Z = \frac{1}{T(j\omega)^P} \quad [38]$$

where Z is impedance, T is the time constant, *j* is the imaginary number, ω is the angular frequency of the AC signal, and the exponent P refers to the line produced on the complex-plane, for example a P=0.5 would generate a 45 ° line on the Nyquist plot. The Rp component is the polarization resistance value of the working electrode. The higher the polarization resistance, in this case, the better the sample is at resisting corrosion.

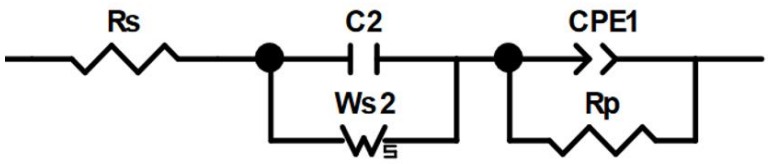

Figure 31. Equivalent circuit model for finite-length diffusion systems.

The ZView results when fitting Figure 31 onto the experimental data for all alloys tested here starts at Table 26. Nickel EIS modeling showed chi-squared values ranging from 0.004 to 0.006 and sum of squared error values ranging from 0.45 to 0.73 in data taken over a 4-hour period. The Inconel 600 wire EIS model showed chi-squared values from 0.006 to 0.01 and sum of square values ranging from 0.68 to 1.25 over a 4-hour period. SS308 wire EIS modeling showed chi-squared error values ranging from 0.006 to 0.01 and sum of squared error values from 0.75 to 1.15 over a 4-hour period. SS304 EIS modeling showed chi-squared error values ranging from 0.007 to 0.009 and sum of squared error values ranging from 0.7 to 1 in data taken over a duration of 5 hours. HastelloyN EIS modeling showed chi-squared error values ranging from 0.002 to 0.004 and sum of squared error values ranging from 0.23 to 0.44. Inconel 617 EIS modeling showed chi-squared error values ranging from 0.003 to 0.005 and sum of squared error values ranging from 0.35 to 0.55. Inconel 600 EIS modeling showed chi-squared error values ranging from 0.002 to 0.004 and sum of squared error values ranging from 0.19 to 0.44.

The chi-squared error value here is defined as the square of the standard deviation between the original data and the calculated data where a typical decent fit value will be seen as 100 or less. The actual value obtained from the chi-square error modeling has been historically scrutinized[39] since it provides an error with a value. For example, if the chi-square error value is 1, applying the error to a value of 1000 shows a 0.1% error but applying it to a similar value of 1 returns a 50% error. The need to include a second type of fitting result was added to the modeling process, which is the sum of squares (sum-sqr). Sum of squares is proportional to the average percentage error between the experimental data and that which was calculated. Both error values from the modeling process are

utilized when criticizing models. The error values obtained for using the RsL[CPE-Rp][C-Ws] circuit on the alloys shows very low errors from both goodness of fit methods.

The limitations of using the CPE[40] should also be mentioned since a CPE was used in this model. As the CPE allows more freedom during modeling, it tends to fit data a lot better where a normal capacitor would, and should, fit instead. There are two major limitations to consider when using a CPE. The first major limitation involves assuming that the time constant for the CPE is distributed and not a single value as not all systems follow the specific distribution method for the CPE equation mentioned above. The second major limitation is that one should not assume that just because the CPE fits the data means that it is describing the physical processes in the system because impedance models are not known to be unique therefore the CPE may not provide adequate physical representation.

A caveat to using this model over the preferred model is that the error in some physical properties goes up but you gain the ability to model diffusion coefficients and diffusion layer thicknesses. This model should not be utilized for strictly determining corrosion mechanisms and properties of the materials but is best suited for further electrochemical engineering applications that require diffusion coefficients and diffusion layer thicknesses.

Table 26. Nickel EIS

Hrs	0.5	1	2	4
Chi-Sqr	0.004309	0.006484	0.004501	0.004014
Sum-Sqr	0.48689	0.73269	0.50862	0.45353
Rs(+)	2.295	2.407	2.347	2.344
Rs(Error)	0.050771	0.063803	0.048193	0.047751
Rs(Error%)	2.2122	2.6507	2.0534	2.0372
CPE1-T(+)	0.000669	0.000876	0.000912	0.000826
CPE1-	4.23E-05	0.000104	9.39E-05	6.71E-05
CPE1-	6.3219	11.838	10.292	8.12
CPE1-P(+)	0.83783	0.82129	0.87144	0.85191
CPE1-	0.053746	0.10172	0.10227	0.086984
CPE1-	6.4149	12.385	11.736	10.21
Rp(+)	3415	2071	2109	2640
Rp(Error)	584.99	499.64	503.55	593.23
Rp(Error%)	17.13	24.126	23.876	22.471
C1(+)	4.70E-05	3.86E-05	3.05E-05	2.87E-05
C1(Error)	9.50E-06	8.06E-06	4.69E-06	4.27E-06
C1(Error%)	20.24	20.909	15.393	14.893
Ws1-R(+)	298.5	251.2	345.4	333.6
Ws1-	61.68	87.262	91.427	81.388
Ws1-	20.663	34.738	26.47	24.397
Ws1-T(+)	0.21229	0.20837	0.27506	0.24384
Ws1-	0.048729	0.072396	0.065299	0.054027
Ws1-	22.954	34.744	23.74	22.157
Ws1-P(+)	0.45313	0.42388	0.42541	0.43398
Ws1-	0.021256	0.027464	0.023662	0.020637
Ws1-	4.6909	6.4792	5.5622	4.7553

Table 27. Inconel 600w EIS

Hrs	0.5	1	2	4
Chi-Sqr	0.006765	0.011087	0.00607	0.010973
Sum-Sqr	0.76447	1.2528	0.68586	1.2399
Rs(+)	2.251	2.402	2.251	2.274
Rs(Error)	0.053828	0.073853	0.056938	0.067303
Rs(Error%)	2.3913	3.0746	2.5295	2.9597
CPE1-T(+)	0.003725	0.003543	0.003772	0.004278
CPE1-	0.000612	0.000586	0.000426	0.000791
CPE1-	16.42	16.526	11.29	18.499
CPE1-P(+)	0.81676	0.81057	0.78308	0.82116
CPE1-	0.16182	0.17722	0.13379	0.2109
CPE1-	19.812	21.864	17.085	25.683
Rp(+)	544	563.6	629	664.4
Rp(Error)	214.5	252.28	255.78	391.58
Rp(Error%)	39.43	44.762	40.665	58.937
C1(+)	5.04E-05	5.32E-05	4.98E-05	5.88E-05
C1(Error)	1.18E-05	1.49E-05	1.30E-05	1.16E-05
C1(Error%)	23.359	28.07	26.197	19.717
Ws1-R(+)	81.16	70.89	69.74	86.68
Ws1-R(Error)	39.496	40.439	28.923	45.583
Ws1-	48.664	57.045	41.473	52.588
Ws1-T(+)	0.29375	0.22664	0.22409	0.28398
Ws1-T(Error)	0.13146	0.12733	0.086484	0.16987
Ws1-	44.752	56.182	38.593	59.818
Ws1-P(+)	0.38214	0.38892	0.39261	0.37309
Ws1-P(Error)	0.042966	0.046207	0.032776	0.039962
Ws1-	11.244	11.881	8.3482	10.711

Table 28. SS308 EIS

Hrs	0.5	1	2	4
Chi-Sqr	0.008062	0.010206	0.008339	0.006633
Sum-Sqr	0.91105	1.1533	0.94226	0.74948
Rs(+)	1.78	1.799	1.81	1.7
Rs(Error%)	2.2937	2.8033	2.4212	2.0898
CPE1-T(+)	0.007939	0.007068	0.009306	0.011334
CPE1-	39.187	19.375	28.33	34.732
CPE1-P(+)	0.9029	0.82738	0.90668	0.85363
CPE1-	32.668	24.646	29.235	34.059
Rp(+)	321.5	336.9	265.8	273.1
Rp(Error%)	68.507	54.417	78.766	73.592
C1(+)	0.000176	0.000145	0.000137	0.000284
C1(Error%)	26.298	27.595	24.51	23.115
Ws1-R(+)	79.24	49.48	68.08	67.76
Ws1-	60.994	55.768	51.119	47.001
Ws1-T(+)	0.65368	0.29029	0.46695	0.50736
Ws1-	49.292	60.157	53.909	44.531
Ws1-P(+)	0.39674	0.37515	0.37996	0.38318
Ws1-	16.27	11.794	12.661	10.034

Table 29. EIS equivalent circuit model values and error for stainless steel 304 in the 700 °C FLiNaK ingot

Hrs	0.5	1	2	4	5
Chi-Sqr	0.006551	0.008073	0.009201	0.007815	0.009223
Sum-Sqr	0.74023	0.91223	1.0397	0.88307	1.0421
Rs(+)	2.471	2.426	2.311	2.393	2.444
Rs(Error)	0.047625	0.049211	0.0486	0.046988	0.051903
Rs(Error%)	1.9274	2.0285	2.103	1.9636	2.1237
CPE1-T(+)	0.019122	0.022121	0.039319	0.024527	0.024664
CPE1-T(Error)	0.008323	0.027027	0.054543	0.033631	0.040111
CPE1-	43.524	122.18	138.72	137.12	162.63
CPE1-P(+)	0.85479	0.83471	0.93302	0.93781	0.92511
CPE1-P(Error)	0.34081	0.62174	0.9886	0.65472	0.84641
CPE1-	39.871	74.486	105.96	69.814	91.493
Rp(+)	150.7	171.6	123.5	86.34	112.1
Rp(Error)	143.25	230.08	355.84	140.28	218.62
Rp(Error%)	95.056	134.08	288.13	162.47	195.02
C1(+)	0.000241	0.00029	0.000431	0.0003	0.000294
C1(Error)	7.92E-05	9.94E-05	0.000152	7.83E-05	7.60E-05
C1(Error%)	32.918	34.246	35.272	26.125	25.86
Ws1-R(+)	35.48	54.55	59.66	63.24	81.77
Ws1-R(Error)	25.065	62.801	53.838	58.287	75.607
Ws1-	70.645	115.13	90.241	92.168	92.463
Ws1-T(+)	0.60172	1.278	1.42	0.84596	0.93035
Ws1-T(Error)	0.40173	1.4795	1.0307	1.0095	1.0869
Ws1-	66.764	115.77	72.585	119.33	116.83
Ws1-P(+)	0.36321	0.33344	0.36735	0.34212	0.34769
Ws1-P(Error)	0.067857	0.10345	0.10145	0.074947	0.074013
Ws1-P(Error%)	18.683	31.025	27.617	21.907	21.287

Table 30. EIS equivalent circuit model values and error for HastelloyN in the 700 °C FLiNaK ingot

Hrs	0.5	1	2	4	5
Chi-Sqr	0.021523	0.002461	0.002731	0.003728	0.003873
Sum-Sqr	2.4321	0.27812	0.30863	0.42131	0.43761
Rs(+)	12.75	4.855	4.823	4.648	4.638
Rs(Error)	0.40657	0.072016	0.078518	0.080759	0.083595
Rs(Error%)	3.1888	1.4833	1.628	1.7375	1.8024
CPE1-T(+)	0.004127	0.003461	0.003506	0.003872	0.003943
CPE1-	0.005068	0.00025	0.000363	0.000428	0.001098
CPE1-	122.8	7.2146	10.361	11.057	27.833
CPE1-P(+)	0.73821	0.70957	0.71634	0.74236	0.75263
CPE1-P(Error)	0.70628	0.081429	0.10149	0.12487	0.21343
CPE1-	95.675	11.476	14.168	16.821	28.358
Rp(+)	734.6	639.7	613.6	600.4	541.7
Rp(Error)	1170.1	155.69	175.62	194.83	278.91
Rp(Error%)	159.28	24.338	28.621	32.45	51.488
C1(+)	5.51E-05	3.89E-05	4.13E-05	2.68E-05	2.43E-05
C1(Error)	6.47E-05	8.11E-06	1.16E-05	4.77E-06	6.91E-06
C1(Error%)	117.59	20.852	28.004	17.831	28.446
Ws1-R(+)	89.49	57.69	62.25	93.94	131.6
Ws1-R(Error)	229.29	19.292	27.635	29.04	66.346
Ws1-	256.22	33.441	44.394	30.913	50.415
Ws1-T(+)	0.45077	0.14191	0.22174	0.21745	0.44533
Ws1-T(Error)	1.2906	0.058299	0.10468	0.068716	0.18577
Ws1-	286.31	41.082	47.208	31.601	41.715

Table 30 continued

Ws1-P(+)	0.33111	0.35401	0.34161	0.36078	0.3496
Ws1-P(Error)	0.17089	0.022072	0.033799	0.023557	0.049066
Ws1-	51.611	6.2349	9.894	6.5295	14.035

Table 31. EIS equivalent circuit model values and error for Inconel 617 in the 700 °C FLiNaK ingot.

Hrs	0.5	1	2	4	5
Chi-Sqr	0.00416	0.003118	0.003874	0.004902	0.004099
Sum-Sqr	0.47012	0.35234	0.43775	0.55396	0.46316
Rs(+)	5.137	4.379	4.375	4.173	4.089
Rs(Error)	0.089133	0.061701	0.070761	0.08215	0.069942
Rs(Error%)	1.7351	1.409	1.6174	1.9686	1.7105
CPE1-T(+)	0.008783	0.008779	0.00793	0.007423	0.007472
CPE1-	0.001204	0.001401	0.001311	0.001297	0.001301
CPE1-	13.703	15.956	16.528	17.479	17.41
CPE1-P(+)	0.69365	0.75559	0.74863	0.70583	0.75587
CPE1-P(Error)	0.14406	0.15248	0.16551	0.17581	0.17524
CPE1-	20.768	20.18	22.108	24.908	23.184
Rp(+)	363.8	358.2	398	537.8	453.8
Rp(Error)	178.95	167.69	214.38	354.03	265.89
Rp(Error%)	49.189	46.815	53.864	65.829	58.592
C1(+)	0.000171	0.000177	1.29E-04	8.53E-05	7.84E-05
C1(Error)	9.47E-05	7.00E-05	5.77E-05	4.54E-05	3.05E-05
C1(Error%)	55.442	39.624	44.656	53.183	38.868
Ws1-R(+)	23.2	36.48	35.84	35.17	45.69
Ws1-R(Error)	16.582	19.545	22.945	25.07	25.629
Ws1-	71.474	53.577	64.021	71.282	56.093
Ws1-T(+)	0.27857	0.47082	0.41413	0.42069	0.48059
Ws1-T(Error)	0.15627	0.20029	0.22861	0.25335	0.23962
Ws1-	56.097	42.541	55.202	60.222	49.86
Ws1-P(+)	0.38002	0.37501	0.36808	0.37438	0.37788
Ws1-P(Error)	0.039263	0.043899	0.053746	0.050207	0.051879
Ws1-	10.332	11.706	14.602	13.411	13.729

Table 32. EIS equivalent circuit model values and error for Inconel 600 in the 700 °C FLiNaK ingot.

Hrs	0.5	1	2	4	5
Chi-Sqr	0.003881	0.001986	0.001662	0.00201	0.0022
Sum-Sqr	0.43859	0.22444	0.18781	0.22712	0.24864
Rs(+)	4.493	4.766	4.879	4.624	4.156
Rs(Error)	0.066042	0.058671	0.055196	0.06098	0.049076
Rs(Error%)	1.4699	1.231	1.1313	1.3188	1.1808
CPE1-T(+)	0.005675	0.0048	0.004592	0.00478	0.005518
CPE1-	7.33E-04	3.38E-04	2.80E-04	5.32E-04	1.11E-03
CPE1-	12.912	7.0468	6.1044	11.124	20.173
CPE1-P(+)	0.80374	0.71299	0.72287	0.72243	0.78829
CPE1-P(Error)	0.11604	0.072825	0.074825	0.11865	0.16082
CPE1-	14.438	10.214	10.351	16.424	20.401
Rp(+)	487.8	609.2	722.5	798.7	6.58E+02
Rp(Error)	167.36	146.7	206.82	364.13	3.41E+02
Rp(Error%)	34.309	24.081	28.626	45.59	51.769
C1(+)	0.000335	0.000167	8.66E-05	5.84E-05	6.20E-05
C1(Error)	0.000108	5.99E-05	2.47E-05	2.17E-05	1.94E-05
C1(Error%)	32.297	35.949	28.532	37.175	31.218
Ws1-R(+)	61.24	31.75	38.02	50.3	78.2

Table 32 continued.

Ws1-R(Error)	21.697	13.819	15.099	28.052	43.507
Ws1-	35.429	43.524	39.713	55.769	55.636
Ws1-T(+)	0.31108	0.22433	0.26267	0.44606	0.94651
Ws1-T(Error)	0.12096	0.086501	0.092881	0.23113	0.62918
Ws1-	38.884	38.56	35.36	51.816	66.474
Ws1-P(+)	0.39887	0.39086	0.36932	0.34883	0.3428
Ws1-P(Error)	0.029663	0.024635	0.028475	0.050794	0.064257
Ws1-	7.4368	6.3028	7.7101	14.561	18.745

References

1. L. Mathieu, D. Heuer, E. Merle-Lucotte et al., Possible Configurations for the Thorium Molten Salt Reactor and Advantages of the Fast Non-Moderated Version, Nucl. Sc. and Eng., 161, 78-89 (2009).
2. Lane, James A. Fluid Fuel Reactors. Reading, MA: Addison-Wesley Pub, 1958, p. 574
3. L. C. Olson et al., Journal of Solar Energy Engineering, 137, 061007 (2015).
4. Chakri, S., I. Frateur, M.E. Orazem, E.M.M. Sutter, T.T.M. Tran, B. Tribollet, and V. Vivier. "Improved EIS Analysis of the Electrochemical Behaviour of Carbon Steel in Alkaline Solution." Electrochimica Acta 246 (August 2017): 924–30. https://doi.org/10.1016/j.electacta.2017.06.096.
5. Usman, B. J., F. Scenini, and M. Curioni. "Corrosion Testing of Anodized Aerospace Alloys: Comparison Between Immersion and Salt Spray Testing Using Electrochemical Impedance Spectroscopy." Journal of The Electrochemical Society 167, no. 4 (January 3, 2020): 041505. https://doi.org/10.1149/1945-7111/ab74e3.
6. Encinas-Sánchez, V., M.T. de Miguel, M.I. Lasanta, G. García-Martín, and F.J. Pérez. "Electrochemical Impedance Spectroscopy (EIS): An Efficient Technique for Monitoring Corrosion Processes in Molten Salt Environments in CSP Applications." Solar Energy Materials and Solar Cells 191 (March 2019): 157–63. https://doi.org/10.1016/j.solmat.2018.11.007.
7. Shi, Y.Y., Z. Zhang, J.X. Su, and J.Q. Zhang. "EIS Study on 2024-T3 Aluminum Alloy Corrosion in Simulated Acid Rain under Cyclic Wet-Dry Conditions." Materials and Corrosion 56, no. 10 (October 2005): 701–6. https://doi.org/10.1002/maco.200503869.
8. Zhou, Wentao, and Jinsuo Zhang. "Chemical Diffusion Coefficient Calculation of U3+ in LiCl-KCl Molten Salt." *Progress in Nuclear Energy* 91 (August 2016): 170–74. https://doi.org/10.1016/j.pnucene.2016.04.017.
9. Ehsani, Ali, Mohammad Ghasem Mahjani, and Majid Jafarian. "Graphite in Basic Molten Salt," n.d., 9.
10. Hua Ai, Xiang-Xi Ye, Li Jiang, Bin Leng, Miao Shen, Zhijun Li, Yanyan Jia, et al. "On the Possibility of Severe Corrosion of a Ni-W-Cr Alloy in Fluoride Molten Salts at High Temperature." Corrosion Science 149 (2019): 218–25.
11. Madjid Sarvghad, Theodore A. Steinberg, and Geoffrey Will. "Corrosion of Stainless Steel 316 in Eutectic Molten Salts for Thermal Energy Storage." Solar Energy 172 (2018): 198–203.

12. Yanli Wang, Huijun Liu, Guojun Yu, and Chaoliu Zeng. “Electrochemical Study of the Corrosion of a Ni-Based Alloy GH3535 in Molten (Li, Na,K)F at 700 C.” Journal of Fluorine Chemistry 178 (2015): 14–22.
13. Ming Zhu, Song Zeng, huihui Zhang, Junyi Li, and Boyuan Cao. “Electrochemical Study on the Corrosion Behaviors of 316 SS in HITEC Molten Salt at Different Temperatures.” Solar Enegy Materials and Solar Cells 186 (2018): 200–207.
14. J.L. Trinstancho-Reyes, M. Sanchez-Carrillo, R. Sandoval-Jabalera, V.M. Orozco-Carmona, F. Almeraya-Calderon, J.G. Chacon-Nava, J.G. Gonzalez-Rodriguez, and A. Martinez-Villafane. “Electrochemical Impedance Spectroscopy Invesitgation of Alloy Inconel 718 in Molten Salts at High Temperature.” International Journal of Electrochemical Science 6 (2011): 419–31.
15. S J Keny, V K Gupta, A G Kumbhar, S Rangarajan, M R Daitkar, N K Maheshwari, P K Vijayan, and B N Jagatap. “Corrosion Tests of Various Alloys in Fluorides of Lithium, Sodium, and Potassium (FLiNaK) Medium for Molten Salt Reactors in the Temperature Range of 550-750 C Using Electrochemical Techniques.” Indian Journal of Chemical Technology 26 (2019): 84–88.
16. Shaoqiang Guo, Jinsuo Zhang, Wei Wu, and Wentao Zhou. “Corrosion in the Molten Fluoride and Chloride Salts and Materials Development for Nuclear Applications.” Progress in Materials Science 97 (2018): 448–87.
17. Wei Qi, Zhoutong He, Hui Tang, Baoliang Zhang, Can Zhang, Lina Gao, Jinliang Song, et al. “Effects of FLiNaK Infiltration on Thermal Expansion Behavior of Graphite.” J Mater Sci 52 (2017): 4621–34.
18. Mansfeld, Florian. “Tafel Slopes and Corrosion Rates from Polarization Resistance Measurements.” Corrosion 29, no. 10 (January 1, 2013): 397–402. https://doi.org/10.5006/0010-9312-29.10.397.
19. J. Qiu et al., Corrosion Science, 186, 109457 (2021).
20. Impedance Spectroscopy - Theory, Experiment, and Applications, E. Barsoukov and J. R. Macdonald, Editors, 2nd Edition (Wiley-Interscience: New York, NY), 149 (2005)
21. A. E. Danon et al., Corrosion Science, 164, 108306 (2020).
22. C. Montella, Journal of Electroanalytical Chemistry, 879, 114785 (2020).
23. P. Agarwal, M. E. Orazem, and L. H. Garcia-Rubio, J. Electrochem. Soc., 139, 1917–1927 (1992).
24. P. Agarwal, O. D. Crisalle, M. E. Orazem, and L. H. Garcia-Rubio, J. Electrochem. Soc., 142, 4149–4158 (1995).

25. P. Agarwal, M. E. Orazem, and L. H. Garcia-Rubio, J. Electrochem. Soc., 142, 4159–4168 (1995).
26. B. A. Boukamp, J. Electrochem. Soc., 142, 1885–1894 (1995).
27. R. Curtain and K. Morris, Automatica, 45, 1101–1116 (2009).
28. P. Lagonotte, V. A. R. Ilie, S. Martemianov, and A. Thomas, Journal of Electroanalytical Chemistry, 839, 256–263 (2019).
29. M. Schönleber and E. Ivers-Tiffée, Electrochemistry Communications, 58, 15–19 (2015).
30. R. Michel and C. Montella, Journal of Electroanalytical Chemistry, 736, 139–146 (2015).34.
31. J.-P. Diard and C. Montella, Journal of Electroanalytical Chemistry, 742, 37–46 (2015).
32. Impedance Spectroscopy - Theory, Experiment, and Applications, E. Barsoukov and J. R. Macdonald, Editors, 2nd Edition (Wiley-Interscience: New York, NY), 149 (2005)
33. M. E. Orazem and B. Tribollet, Electrochemical impedance spectroscopy, Wiley, Hoboken, N.J, (2008).
34. Niketan S. Patel, Viliam Pavlik, Blanka Kubikova, Martin Nosko, Vladimir Danielik, and Miroslav Boca. “Corrosion Behaviour of Ni-Based Superalloys in Molten FLiNaK Salts.” Corrosion Engineering, Science and Technology, n.d. https://doi.org/10.1080/1478422X.2018.1525829.